54p

N 63 15922

53414

. P-56

Code -1

NASA

TECHNICAL NOTE

D-1884

LARGE-SCALE WIND-TUNNEL TESTS IN GROUND EFFECT OF A

35° SWEPTBACK WING JET TRANSPORT MODEL EQUIPPED

WITH BLOWING BOUNDARY-LAYER-CONTROL TRAILING-

AND LEADING-EDGE FLAPS

By Kiyoshi Aoyagi and David H. Hickey

Ames Research Center
Moffett Field, Calif.

NATIONAL AERONAUTICS AND SPACE ADMINISTRATION

WASHINGTON   May 1963

NATIONAL AERONAUTICS AND SPACE ADMINISTRATION

TECHNICAL NOTE D-1884

LARGE-SCALE WIND-TUNNEL TESTS IN GROUND EFFECT OF A

35° SWEPTBACK WING JET TRANSPORT MODEL EQUIPPED

WITH BLOWING BOUNDARY-LAYER-CONTROL TRAILING-

AND LEADING-EDGE FLAPS

By Kiyoshi Aoyagi and David H. Hickey

SUMMARY

15922

The effect of ground proximity on the longitudinal characteristics of a large-scale subsonic jet transport with a 35° swept wing of aspect ratio 7 was investigated. Two chordwise and spanwise extents of trailing-edge flaps with and without blowing boundary-layer control were tested with the normal wing leading edge. A limited amount of data was obtained with the blowing boundary-layer-control leading-edge flap.

Three-component longitudinal data and boundary-layer-control flow requirements are presented for several heights above ground. Also presented are data showing the effects of ground proximity on the trimmed lift coefficient of the model and on the calculated thrust-to-weight ratio required to maintain low-speed level flight with several trailing-edge flap configurations.

For trailing-edge flap configurations with BLC, the lift coefficient at zero angle of attack generally increased, then decreased below the maximum as the model height above the ground plane decreased. In addition, ground proximity caused a significant reduction in trimmed maximum lift coefficient and a decrease in lift-curve slope at high angles of attack.

INTRODUCTION

The low-speed aerodynamic characteristics of a large-scale typical subsonic jet transport model equipped with effective high-lift devices have been reported in references 1 and 2. As a further extension of the transport studies the present investigation was undertaken to study the effect of ground proximity on the aerodynamic characteristics of this model.

Three-component force and moment data and boundary-layer-control flow requirements are presented for the model at several heights above the ground plane. Several trailing-edge flap variables investigated with the normal wing

leading edge included flap chord, flap deflection, and spanwise extent. A limited amount of data was obtained with the blowing boundary-layer-control leading-edge flap in combination with one trailing-edge flap configuration. Data are presented to show the effect of ground proximity on the trimmed lift curves of the model and on the trimmed lift coefficients at zero angle of attack with several flap configurations. The effect of ground proximity on the variation of calculated thrust-to-weight ratio required to maintain low-speed level flight is also presented. All data were obtained at a Reynolds number of 4.2×10^6.

NOTATION

b   wing span, ft

BLC   boundary-layer control

c   wing chord, measured parallel to the line of symmetry, ft

$\bar{c}$ mean aerodynamic chord, $\dfrac{2}{S}\displaystyle\int_0^{b/2} c^2\,dy$, ft

C_D drag coefficient, $\dfrac{\text{drag}}{q_\infty S}$

C_m pitching moment about $0.30\bar{c}$, $\dfrac{\text{pitching moment}}{q_\infty S \bar{c}}$

C_μ momentum coefficient, $\dfrac{W_j V_j}{g q_\infty S}$

D   drag, lb

GE   ground effect

g   acceleration of gravity, 32.2 ft/sec^2

h   distance from ground plane to the model moment center at $\alpha = 0^\circ$, ft

L   lift, lb

l_t distance between model moment center and quarter-chord point of the horizontal-tail mean aerodynamic chord, ft

q_∞ free-stream dynamic pressure, lb/sq ft

S   wing area, sq ft

T   thrust, lb

V   velocity, knots

V_j jet velocity, assuming isentropic expansion, ft/sec

V_S stalling airspeed, knots

W   gross weight, lb, or weight rate of flow, lb/sec

x   streamwise distance along airfoil chord, ft

y   spanwise distance perpendicular to the plane of symmetry, ft

z   perpendicular distance above the extended wing-chord plane, ft

α angle of attack of fuselage reference line, deg

δ_f trailing-edge flap deflection measured normal to the hinge line

δn leading-edge flap deflection measured normal to the hinge line

η wing semispan station

ρ density, 0.002378 slug/ft^3

Subscripts

j   flap jet

l lower

le leading edge

te   trailing edge

u   upper

MODEL AND APPARATUS

Figure 1 is a photograph of the model in the 40- by 80-foot wind tunnel with the ground plane installation. Pertinent dimensions of the model are given in figures 2 and 3.

Wing

The wing was swept back 35° at the quarter-chord line. It had an aspect ratio of 7, a taper ratio of 0.3, a dihedral of 6°, and an incidence of 2°. The wing had an NACA 65A414 airfoil section at the root, and tapered linearly to a 65A410 section at the tip (see table I for ordinates).

Leading-Edge Flap System

A plain leading-edge flap was hinged at 15-percent chord, and the BLC ducting was contained in the forward 20-percent chord of the wing. The blowing nozzle was located on the flap radius $46\text{-}1/2^\circ$ from the perpendicular to the flap-chord line. A typical leading-edge flap cross section is shown in figure 3(a). Flap breaks at each engine pylon station were provided so that each flap segment could be individually deflected. For this investigation, however, all three flap segments were deflected together.

Air for BLC was provided in the same manner as described in the following sections for the trailing-edge flap except a separate centrifugal pump was used.

Trailing-Edge Flap System

The wing-flap geometry and a typical cross section of the flap are shown in figure 3(b).

Flap details.- The trailing-edge flap used in the investigation is the same one described in reference 2. The plain flap was hinged at 68-percent chord, and the BLC ducting was placed within the flap. The blowing nozzle was located on the flap radius 35° from the perpendicular to the flap-chord line.

The flap was divided into three segments with breaks perpendicular to the hinge line at 34-, 44-, and 63-percent wing semispan at the wing trailing edge. Flap deflections with the flap segment from 34- to 44-percent wing semispan undeflected will be referred to as the interrupted-span flap. When all three segments of the flap are deflected, the flap will be referred to as the continuous-span flap.

To simulate Fowler type flap action, provisions were made to add a 15-percent chord extension beyond the deflected flap trailing edge. The extension was made from a 1/4-inch plywood sheet and was attached directly to the flap upper surface. The flap without the extension will be referred to as a normal flap. With the extension the flap will be referred to as an extended chord flap.

Boundary-layer-control air supply.- Air for BLC was provided by a centrifugal pump driven by electric motors. This unit was installed in the model fuselage. Air from the blower was ducted to a plenum chamber and then by separate ducting to the flap on either side of the fuselage. Each duct to the flap had a calibrated flow measuring station consisting of total head tubes, static orifices, and a thermocouple.

Fuselage

A 4- by 5-foot ellipse comprised the fuselage cross section except at the nose and tail section. The nose section was one-half of a 4- by 8-foot ellipse

in the horizontal cross section and a 5- by 8-foot ellipse in the vertical cross section. The tail section had a straight taper from a 4- by 5-foot ellipse to a smaller ellipse at the tail.

Nacelles and Pylons

Nacelles and pylons could be attached to the wing at 40- and 70-percent wing semispan. The cylindrical nacelles had a diameter of 14 inches and a length of 48 inches, with a conical nose plug 17 inches long. The pylons were 2-1/4 inches thick with faired leading and trailing edges.

The nacelles and pylons were removed when the continuous-span trailing-edge flap was tested.

Tail

Geometry of the horizontal and vertical tails is given in figure 2. Both horizontal and vertical tails were fixed at 0° during the investigation and were on the model throughout the investigation.

TESTING AND PROCEDURE

The distance between the model and the ground plane was varied by raising or lowering the model support struts. Force and moment data were obtained at the model height to wing-span ratios (h/b) of 0.10, 0.15, 0.21, 0.25, and 0.29 (see corrections) through an angle-of-attack range. Clearance between the model and ground plane at h/b = 0.10 limited the angle-of-attack range from -4° to $+12^o$ with the trailing-edge flap deflected 30°. Interference between the trailing-edge flap deflected 50° and the struts limited the angle-of attack range from -4° to $+6^o$ and -4° to $+14^o$ at h/b = 0.10 and 0.15, respectively. With the exceptions noted, data were obtained in most cases through an angle-of-attack range beyond stall.

All tests were conducted at a free-stream airspeed of 93 feet per second, corresponding to a Reynolds number of 4.2×10^6 and a dynamic pressure of 10 pounds per square foot with the model at zero sideslip angle.

Tests With Constant C_μ and Varying Angle of Attack

Two trailing-edge flap spans with and without the chord extensions were tested with the normal wing leading edge at $C_{\mu_{te}}$ values adequate to maintain attached air flow on the trailing-edge flap configurations deflected 30° and 50°. The leading-edge flap deflected 50° was tested at two $C_{\mu_{te}}$ values with the continuous-span normal trailing-edge flap deflected 50°.

5

Tests With Varying C_μ Values at Constant Angle of Attack

Momentum coefficient was varied on both interrupted- and continuous-span trailing-edge flaps, with and without the trailing-edge chord extension, deflected 30° and 50° at 0° angle of attack. The data were obtained with the normal wing leading edge.

CORRECTIONS

The data were corrected for strut tares and wind-tunnel airstream angularity at each of the ground heights tested. No corrections were applied for the effect of wind-tunnel boundaries, except at $h/b = 0.29$. The data at this latter ground height corrected for the effects of the ground plane and wind-tunnel walls are considered in this report to be out of ground effect. The tunnel-wall corrections were as follows:

$\frac{h}{b} = 0.29$ (with ground effect)

$\Delta\alpha = 0.152\ C_L$

$\Delta C_D = 0.00265\ C_L^2$

$\Delta C_m = 0$

$\frac{h}{b} = 0.29$ (out of ground effect)

$\Delta\alpha = 0.66\ C_L$

$\Delta C_D = 0.0115\ C_L^2$

$\Delta C_m = 0.0028\ C_L$

RESULTS

Figures 4 through 8 show the effect of ground proximity on the longitudinal characteristics of the model. Figures 4 and 5 present three-component longitudinal data with the interrupted-span trailing-edge flap having normal and extended chords, respectively. Similarly, figures 6 and 7 present data with the continuous-span trailing-edge flaps having normal and extended chords, respectively. Figure 8 presents data with the leading-edge flap deflected 50° in combination with the continuous-span normal trailing-edge flap deflected 50°.

Figures 9 and 10 show the variation of lift coefficient with momentum coefficient at several heights above ground for the interrupted-span and continuous-span flaps, respectively. Results are presented for both the normal and extended chord flaps at 0° angle of attack.

Figures 11 through 15 show the effect of ground proximity on the trimmed lift coefficient of the model. Figures 11 and 12 present data with the interrupted-span trailing-edge flap having normal and extended chords, respectively. Figures 13 and 14 present data with the continuous-span normal and extended chord trailing-edge flaps, respectively. The data in figures 11 through 14 were obtained with the normal leading edge. Figure 15 presents data for the deflected leading-edge flap with the continuous-span normal flap.

Figures 16 and 17 show the variation with ground proximity of trailing-edge flap effectiveness at $0°$ angle of attack for the interrupted-span and continuous-span flaps, respectively. Results are presented with and without blowing BLC on the trailing-edge flap in combination with the normal leading edge.

Figures 18 and 19 show the variation with velocity of calculated thrust-to-weight ratio required for low-speed level flight at several heights above ground.[1] The results presented in figure 18 are for the interrupted-span flap configurations deflected $50°$ and a wing loading of 65 pounds per square foot.

Similar results at a wing loading of 100 pounds per square foot are presented in figure 19 for the interrupted-span flap configurations deflected $30°$.

DISCUSSION

In the following discussion it should be noted that the term "out of ground effect" refers to data obtained at $h/b = 0.29$ with wind-tunnel wall corrections added. Comparison of these results with similar unpublished results at $h/b = 0.44$ shows only small changes in lift and drag; thus it is believed the corrected longitudinal results at $h/b = 0.29$ are representative of data out of ground effect.

Effect of Ground Proximity on Lift

With the trailing-edge flaps deflected, the effect of ground on the lift coefficient at an angle of attack of $0°$ depended on the flap effectiveness. For the moderately effective flaps without boundary-layer control, the lift coefficient generally increased as the height above ground was reduced. For the more effective flaps with boundary-layer control, the lift coefficient reached a maximum at some height above ground and decreased below the maximum values with further reductions of height above ground. In some cases at high angles of attack, the lift coefficient obtained close to ground with boundary-layer control applied to the trailing-edge flaps was less than values obtained out of ground effect.

---

[1]The data are presented as values of T/W and V, where:

$$\frac{T}{W} = \frac{C_D'}{C_D' \sin \alpha + C_L' \cos \alpha}, \quad V = 0.592 \sqrt{\frac{2}{\rho} \frac{W/S}{(C_L' + C_D' \tan \alpha)}}$$

$$C_L' = C_L + \frac{\overline{c}}{l_t} C_m$$

$$C_D' = C_D + 0.019 \quad \text{(landing gear drag from ref. 2)}$$

The effect of ground proximity on the trimmed maximum lift coefficient was more pronounced for the trailing-edge flap configurations that had higher lift coefficients at low angles of attack. When the flap lift increment was increased either by the chord extension or by boundary-layer control, the ground effect resulted in a significant loss in trimmed maximum lift coefficient.

In general, the lift curves obtained with the trailing-edge flaps deflected showed a parallel shift at low angles of attack and a reduction in slope at high angles of attack as the ground was approached. This was contrary to the increase in the plain wing lift-curve slope with ground proximity predicted by the ground effect theory of reference 3.

Effect of Ground Proximity on Drag

For each trailing-edge flap configuration studied, drag coefficient was reduced substantially at a given lift coefficient as the height above ground was decreased. The drag reductions were sufficiently large to increase lift-to-drag ratios as the ground was approached. The significance of the increase in lift-to-drag ratio is indicated by the decrease in the calculated thrust-to-weight ratio required to maintain low-speed level flight close to the ground, as shown by the curves in figures 18 and 19. These curves are typical for all of the flap configurations tested. The curves indicate improvements in acceleration characteristics on take-off during ground roll and low altitude climbout in the presence of ground effect. With the thrust-to-weight-ratio flight characteristics shown in figure 18, an airplane while landing would tend to float close to the ground as the speed was reduced, from the final approach speed of 1.3 times stall speed, as a result of the increase in lift-to-drag ratio. In some cases with the higher-lift flap configurations, an airplane nearing the ground following the floating period may settle down rapidly because of the loss of lift close to ground. This settling tendency may be overcome if the angle of attack is changed sufficiently to offset the loss in lift.

Ames Research Center
  National Aeronautics and Space Administration
    Moffett Field, Calif., March 18, 1963

REFERENCES

1. Hickey, David H., and Aoyagi, Kiyoshi: Large-Scale Wind-Tunnel Tests of a
    Jet-Transport-Type Model With Leading- and Trailing-Edge High-Lift
    Devices. NACA RM A58H12, 1958.

2. Hickey, David H., and Aoyagi, Kiyoshi: Large-Scale Wind-Tunnel Tests and
    Evaluation of the Low-Speed Performance of a 35° Sweptback Wing Jet
    Transport Model Equipped With a Blowing Boundary-Layer-Control Flap and
    Leading-Edge Slat. NASA TN D-333, 1960.

3. Weiselsberger, C.: Wing Resistance Near the Ground. NACA TM 77, 1922.

Page intentionally left blank
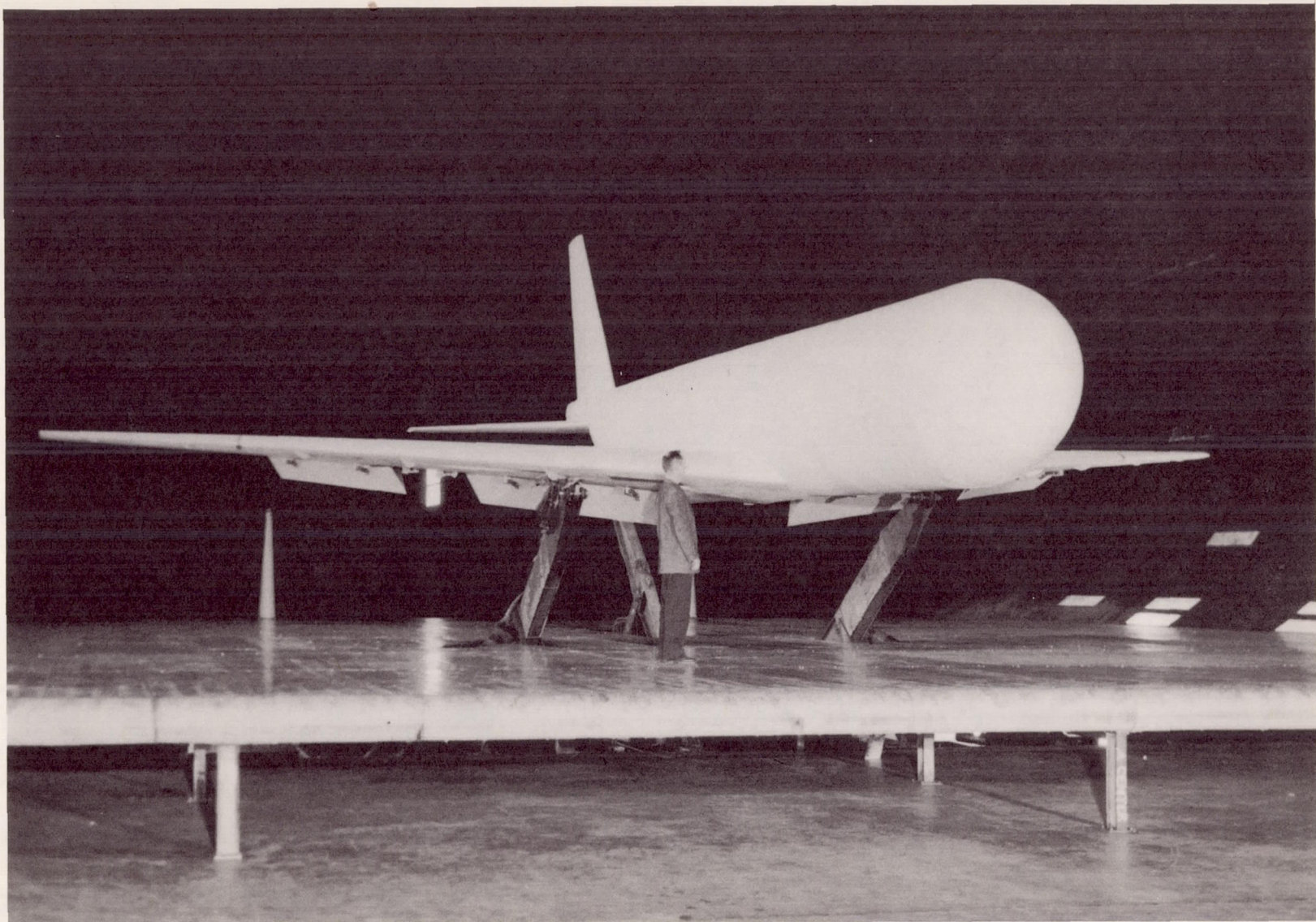
A-29075

Figure 1.- Photograph of model in the Ames 40- by 80-Foot Wind Tunnel.

Moment center

35°

35°

$\overline{c}$

7.67

9.20

9.45

c/4

16.10

21.46

23.00

$\overline{c}$

c/4

All dimensions in feet
except as noted

c/4

9.86

2.07

1.08

2° Wing incidence

.85

h

Ground plane
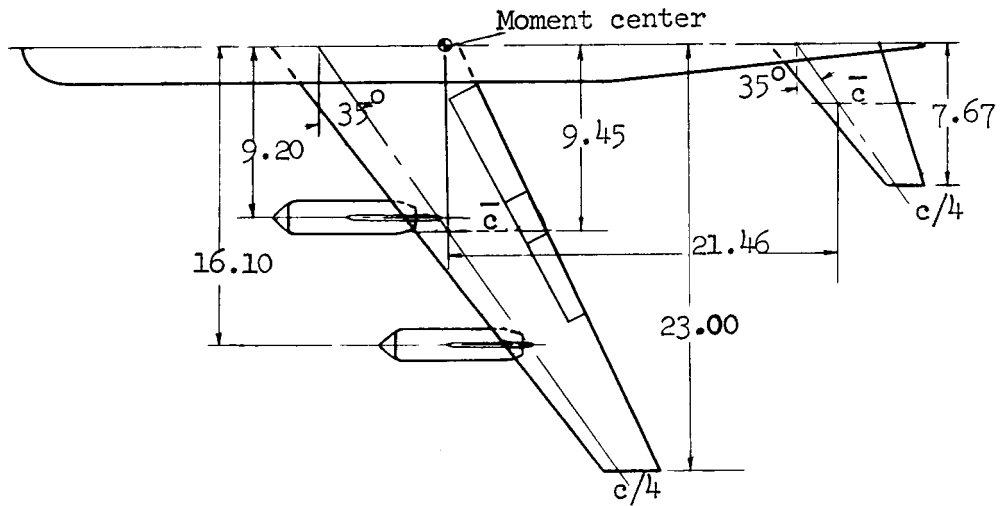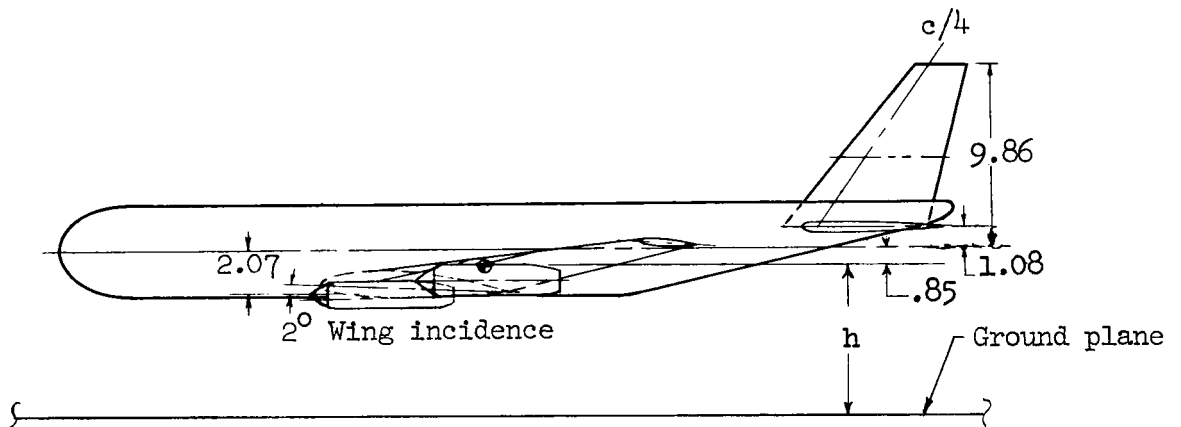
	Wing	Horizontal tail	Vertical tail
Aspect ratio	7.0	3.7	3.3
Taper ratio	0.3	0.375	0.359
Area, sq ft	302.0	62.8	46.7
Mean aerodynamic chord, ft	7.20	4.39	5.72
Dihedral, deg	6.0	0.0	---

Figure 2.- Geometric details of the model.
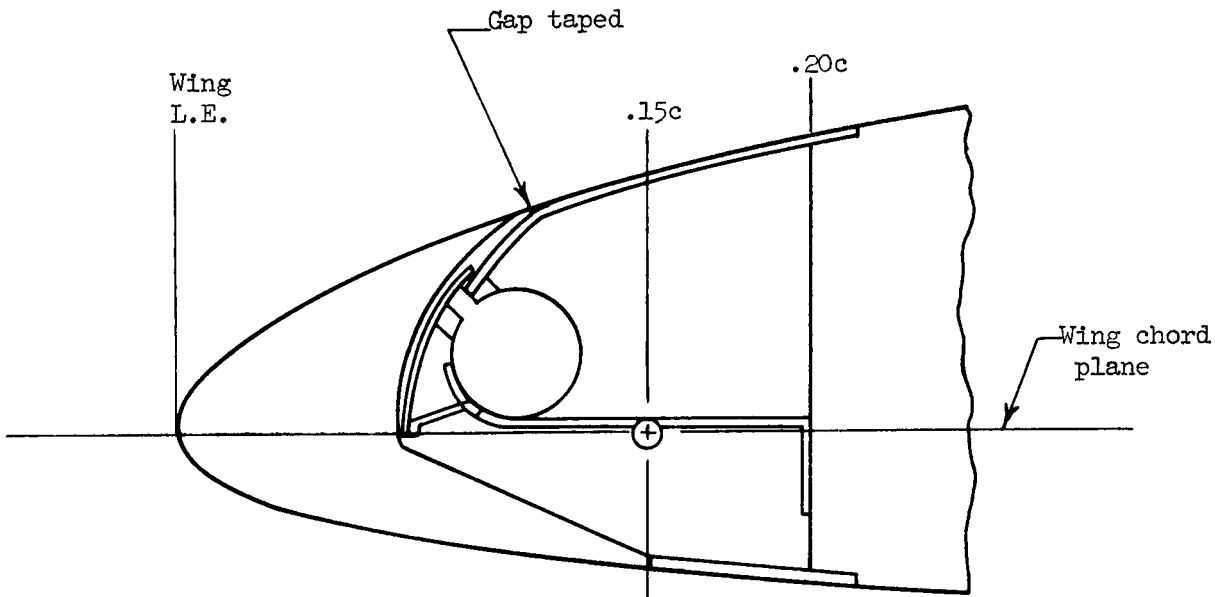
Streamwise airfoil section
  Root   NACA 65A414
  Tip   NACA 65A410
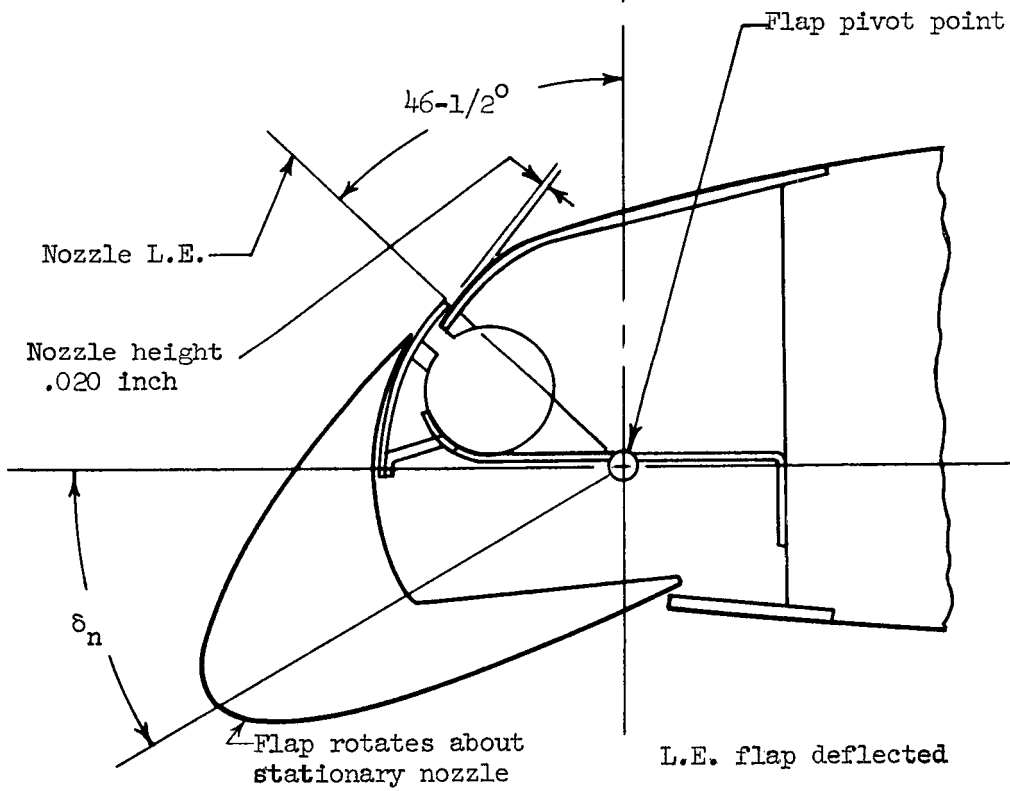
(a) Leading-edge flap (sections perpendicular to 0.15c hinge line).

Figure 3.- Details of the high-lift devices.

Figure content labels:

10.10

29.61°

Fuselage outline

23.00

.4η

.7η

Flap hinge line

.09η

℄ of model

.34η

.44η

A

A

.63η

All dimensions in feet except as noted

3.03

1.0η

.60 c

.68 c

δ_f

35°

Nozzle height, .020 inch

Pivot point of flap

Flap chord line

Detachable chord extension

.32c Normal flap

.15c

Section A-A (typical)
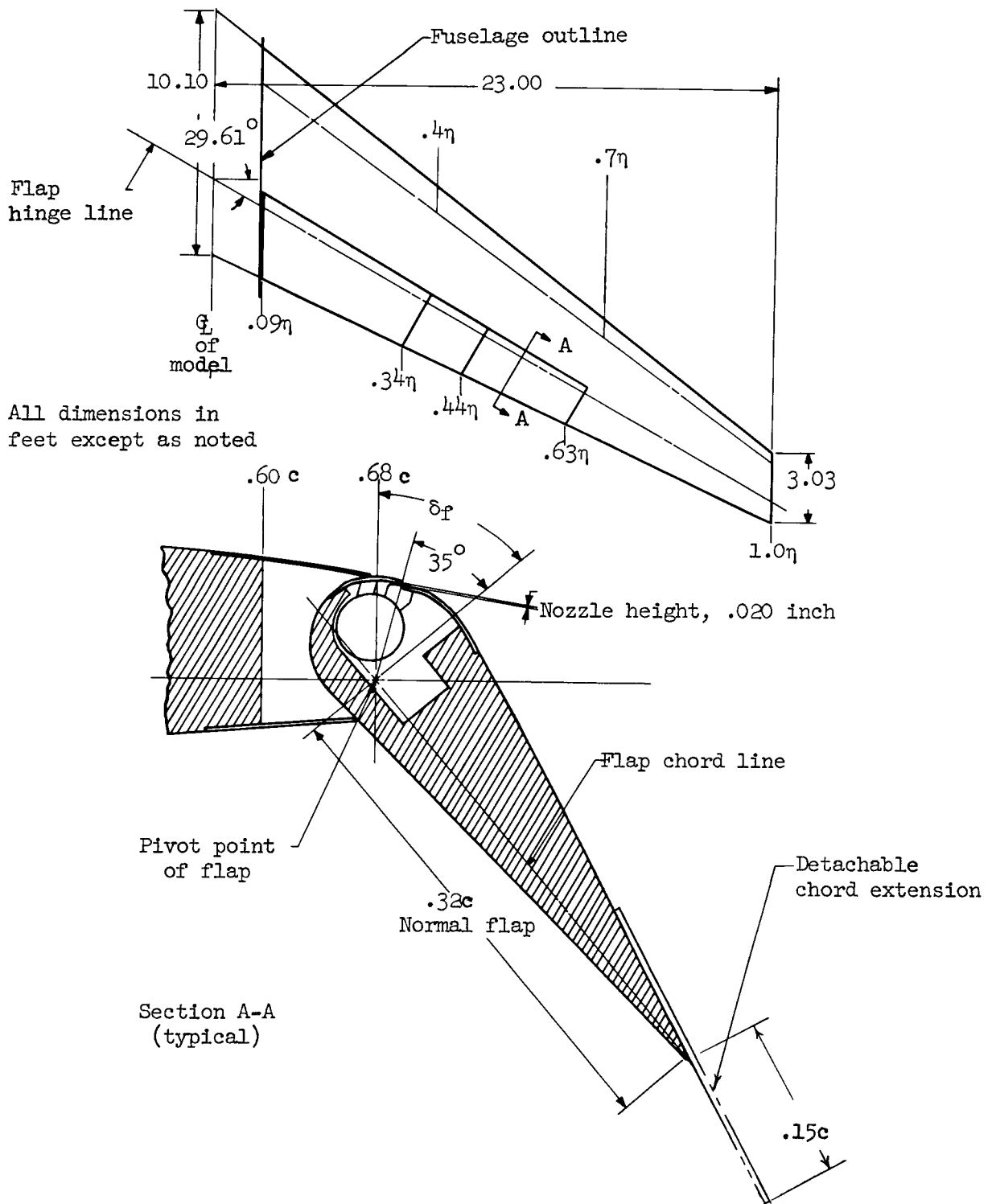
(b) Wing and trailing-edge flap.

Figure 3.- Concluded.
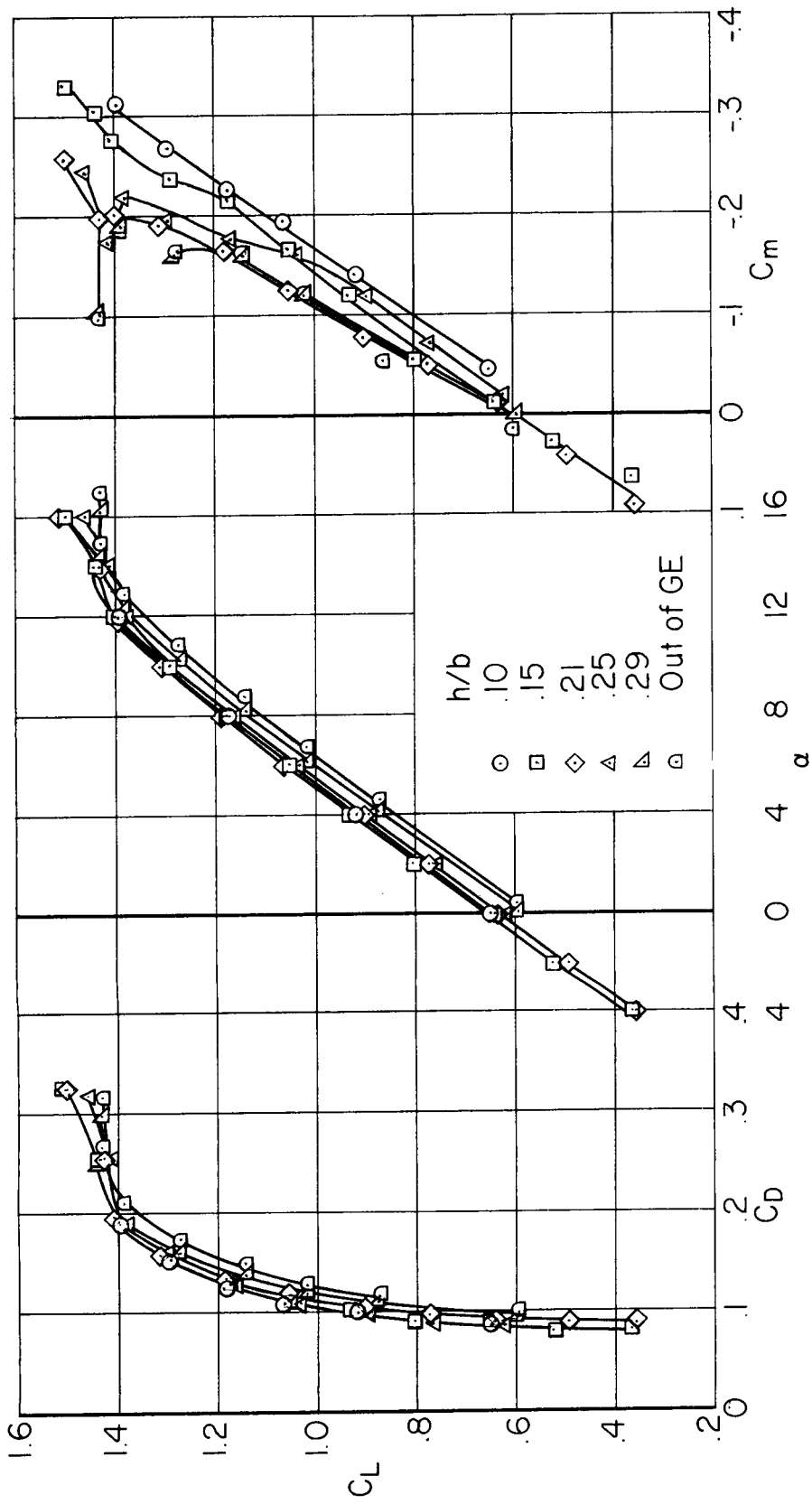
Figure 4.- Effect of ground proximity on the longitudinal characteristics of the model; interrupted-span normal trailing-edge flap, nacelles and pylons on, $\delta_n = 0^\circ$.
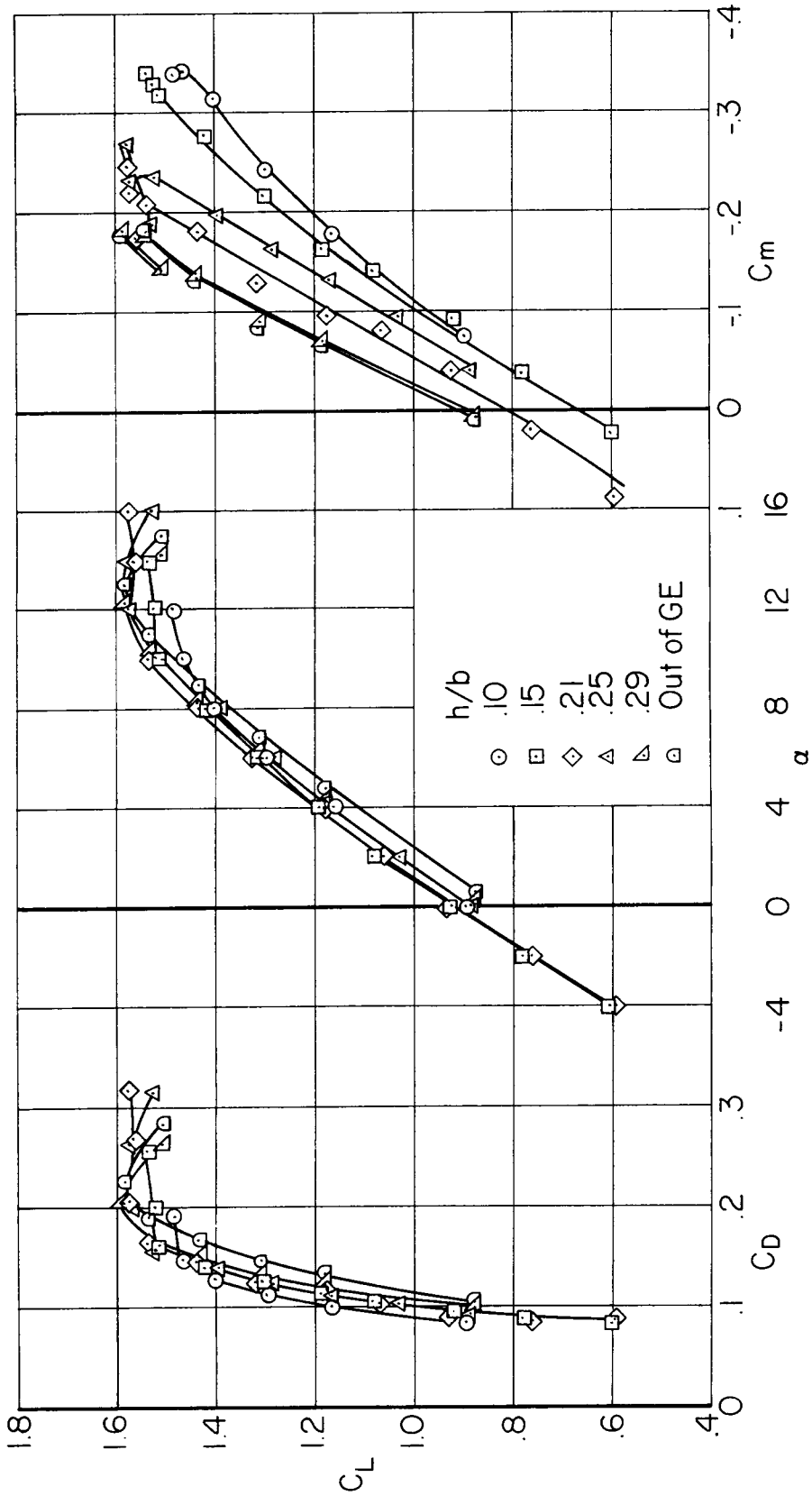
(a) $\delta_f = 30^\circ$, $C_{\mu_{te}} = 0$

(b) $\delta_f = 30°$, $c_{\mu_{te}} = 0.008$

Figure 4.- Continued.
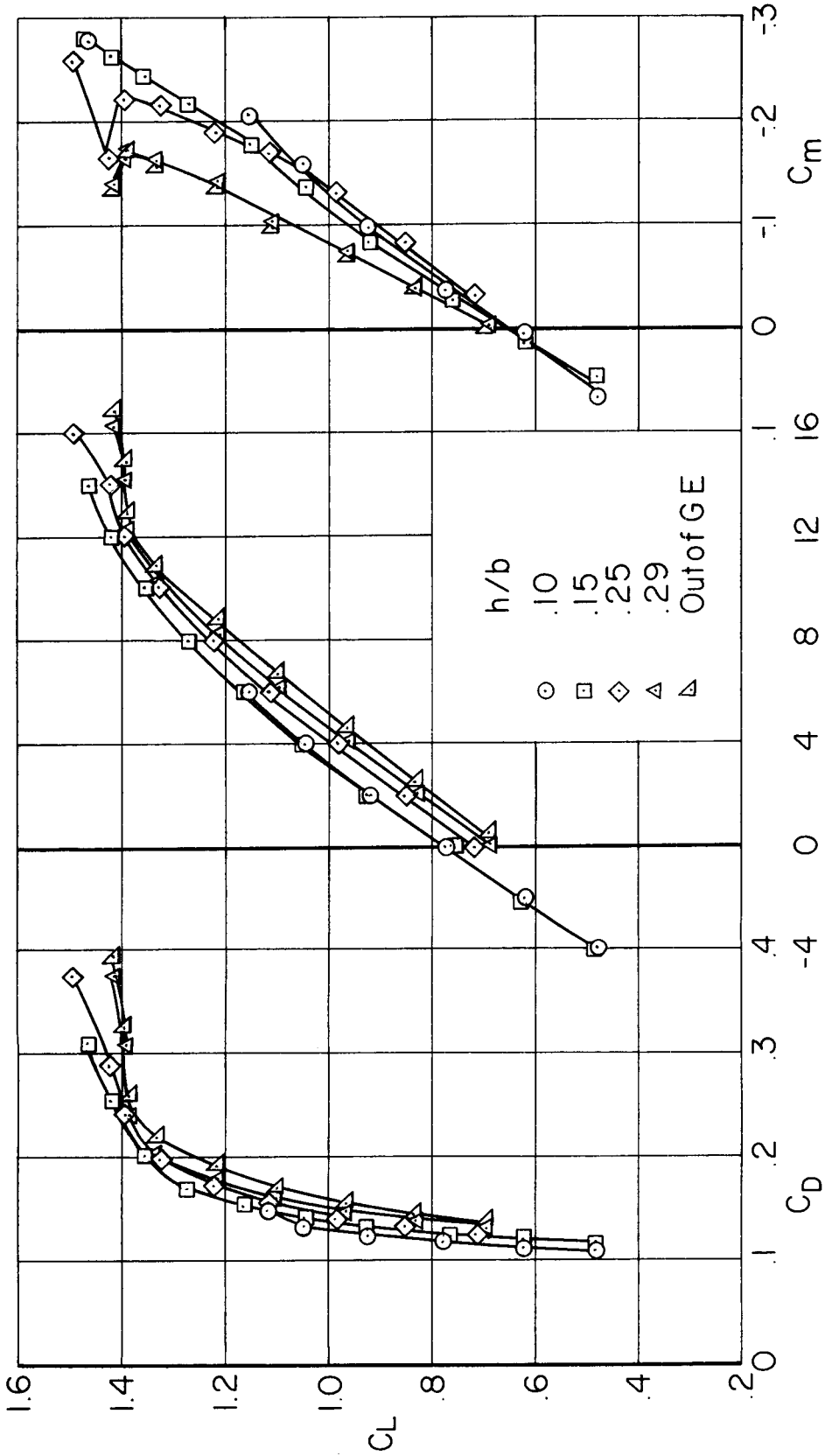
(c) $\delta_f = 50°$, $C_{\mu_{te}} = 0$

Figure 4.- Continued.
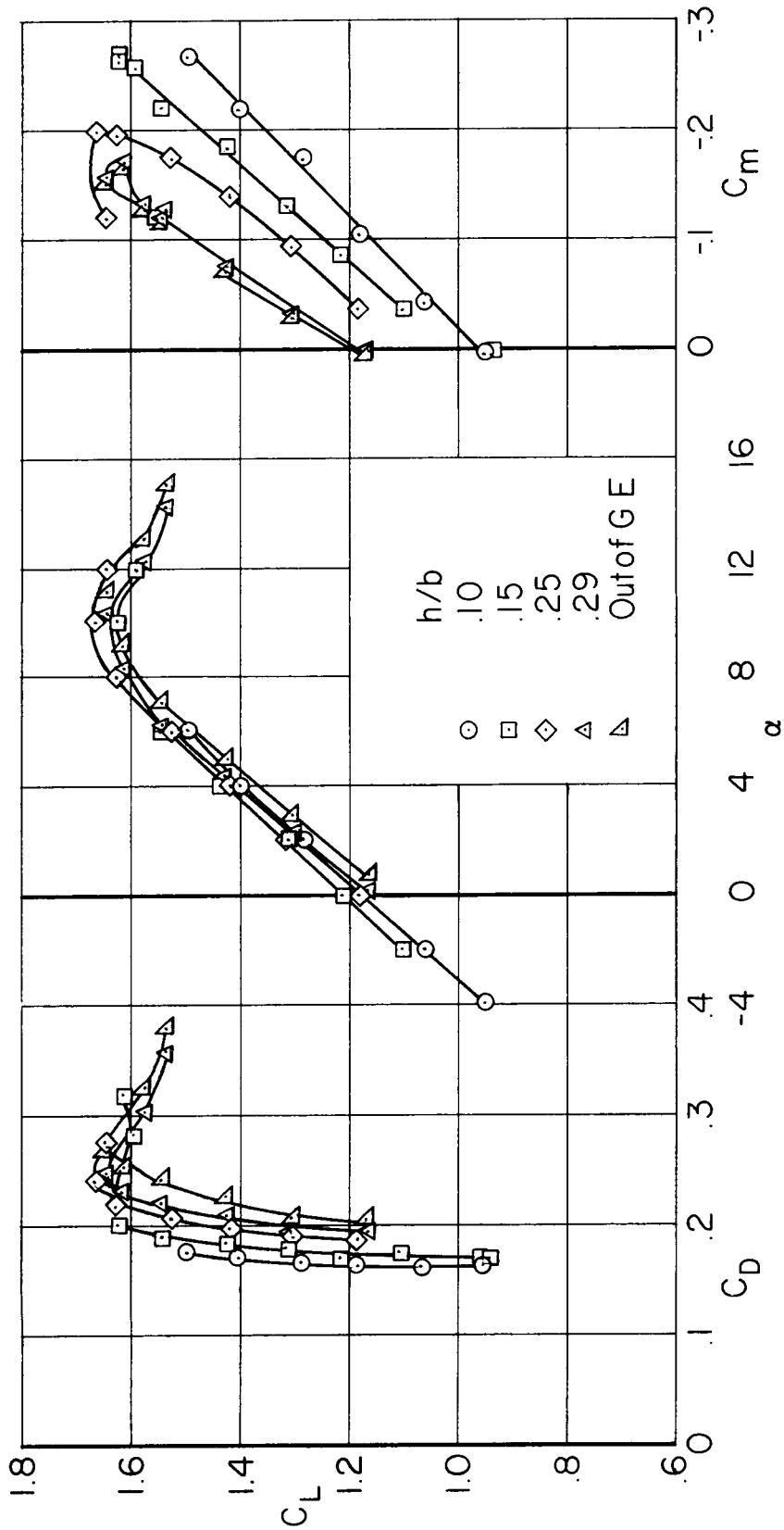
(d) $\delta_f = 50°$, $c_{\mu_{te}} = 0.015$

Figure 4.- Concluded.

18
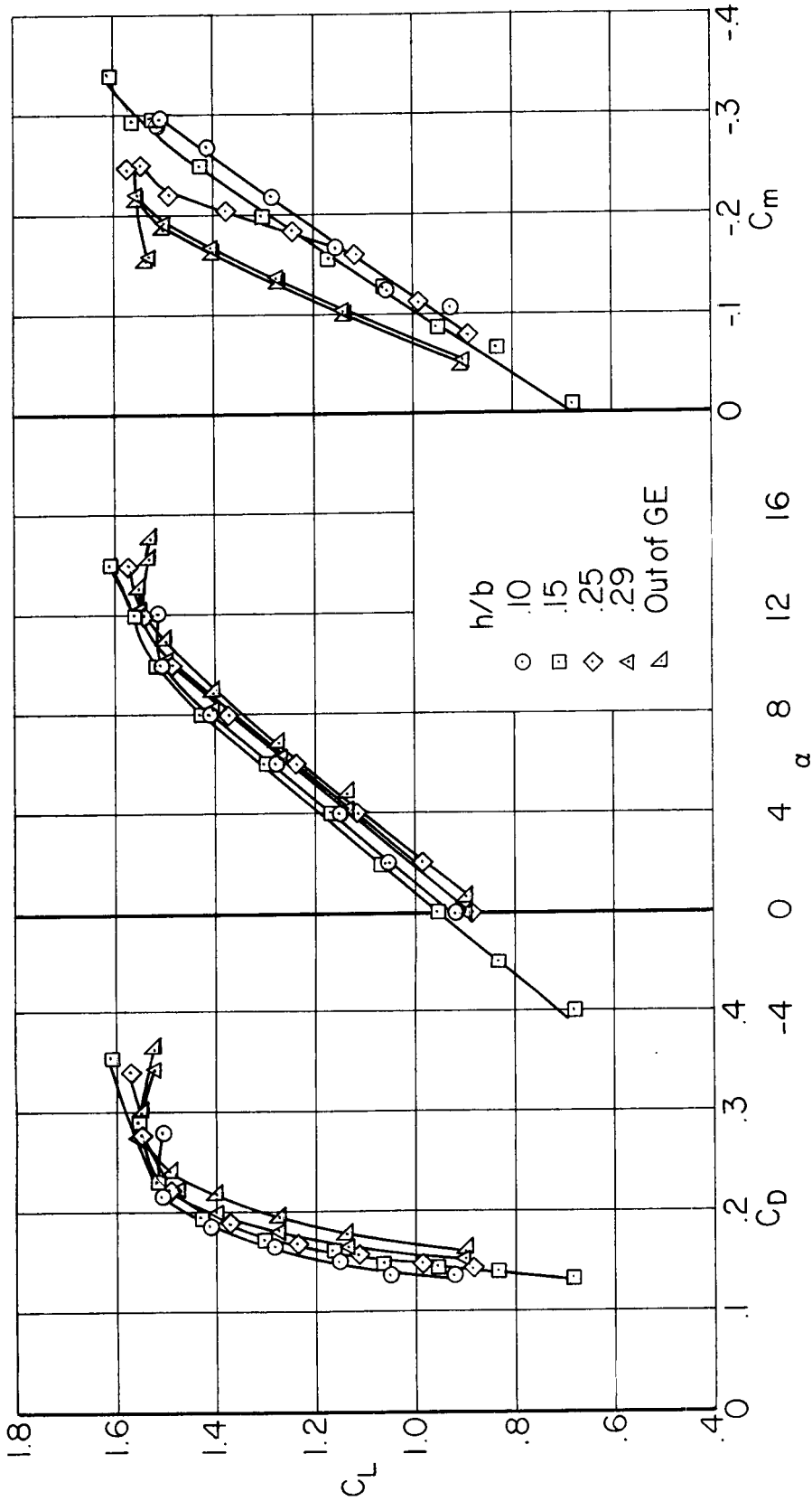
Figure 5.— Effect of ground proximity on the longitudinal characteristics of the model; interrupted-span extended chord trailing-edge flap, nacelles and pylons on, $\delta_n = 0^\circ$.
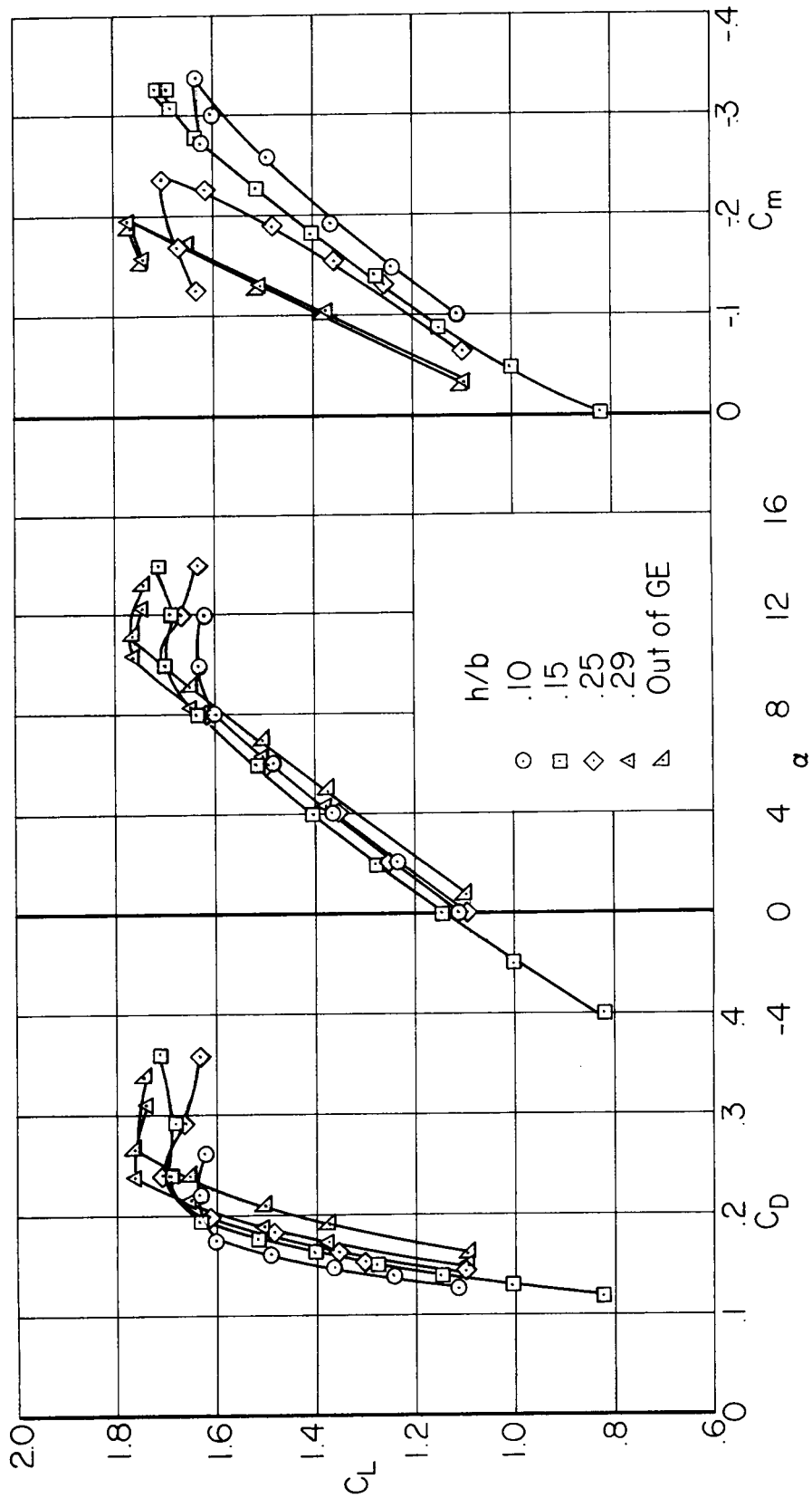
(a) $\delta_f = 30^\circ$, $C_{\mu_{te}} = 0$

(b) $\delta_f = 30°$, $C_{\mu_{te}} = 0.010$

Figure 5.- Continued.
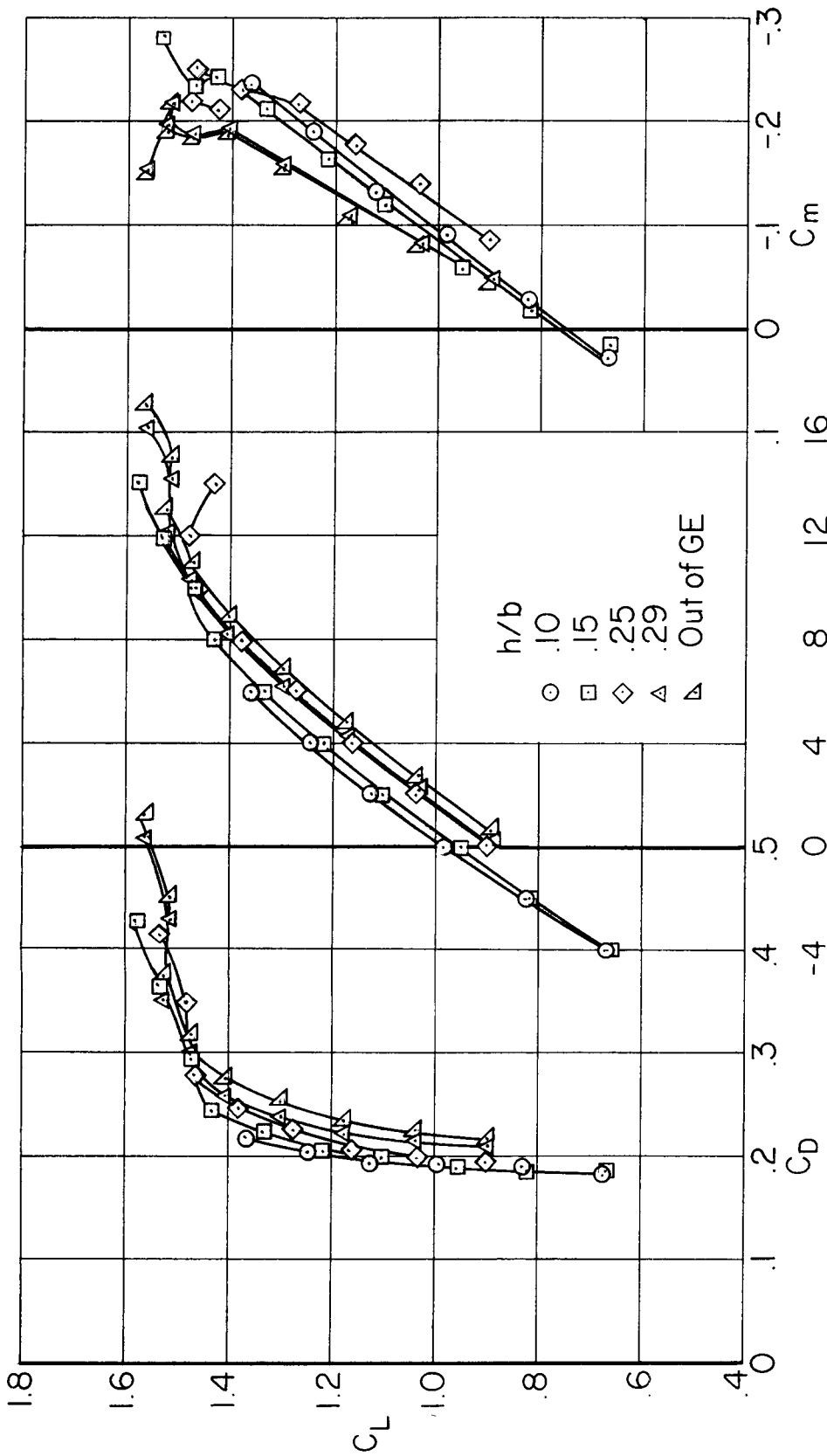
(c) $\delta_f = 50°$, $C_{\mu_{te}} = 0$

Figure 5.— Continued.
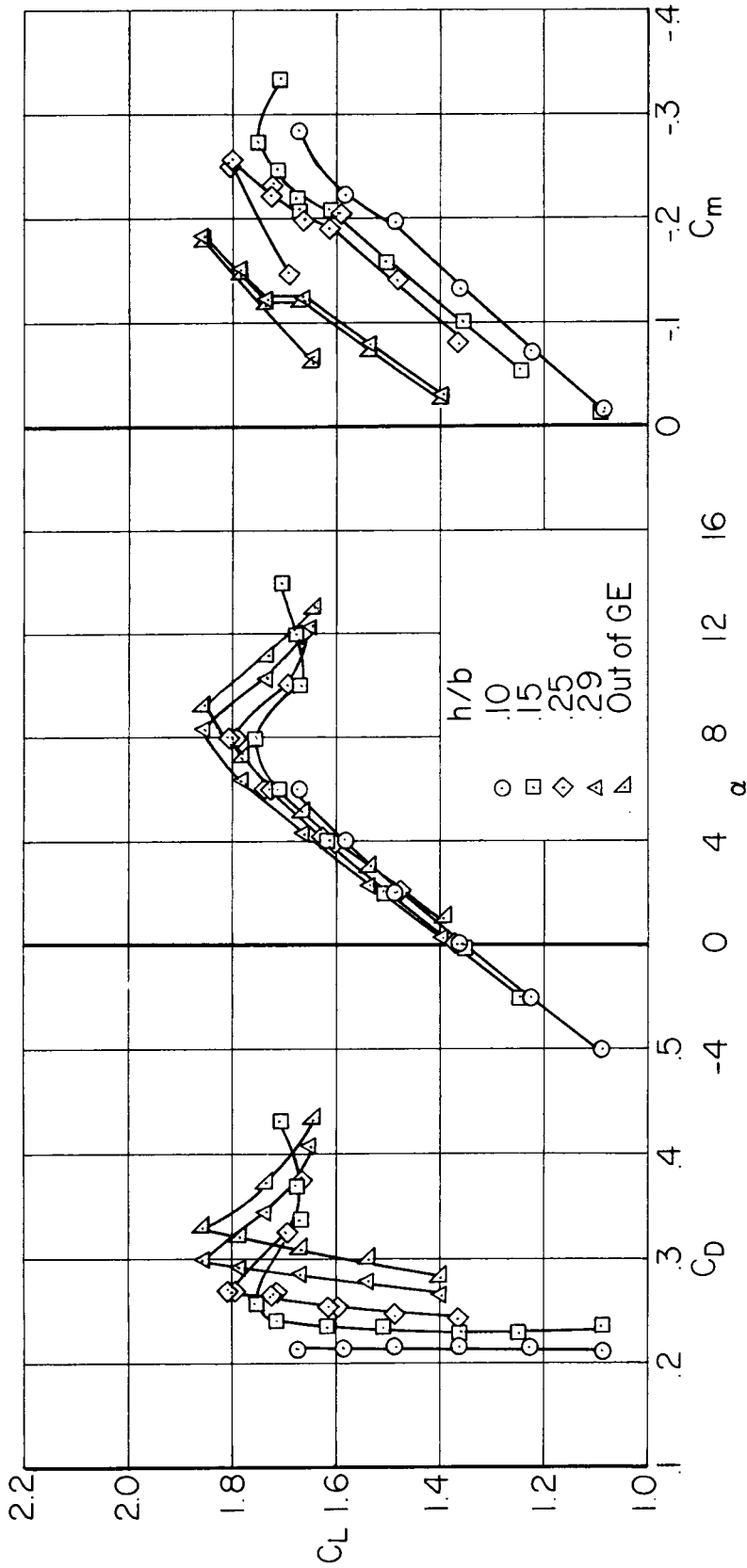
(d) $\delta_f = 50°$, $c_{\mu_{te}} = 0.019$

Figure 5.- Concluded.
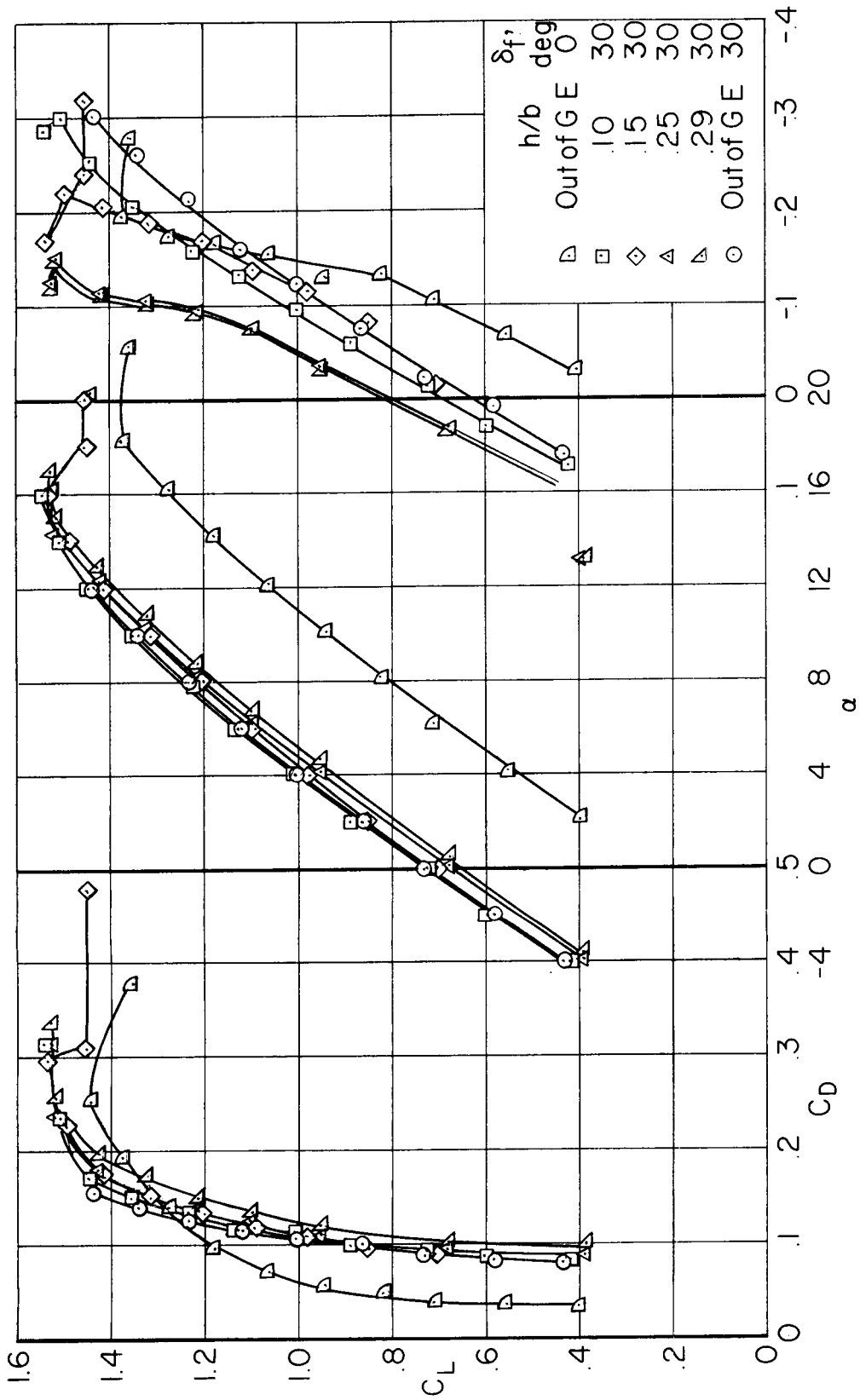
Figure 6.— Effect of ground proximity on the longitudinal characteristics of the model; continuous-span normal trailing-edge flap, nacelles and pylons off, $\delta_n = 0^o$.

(a) $\bar{\delta}_f = 30^o$, $C_{\mu_{te}} = 0$
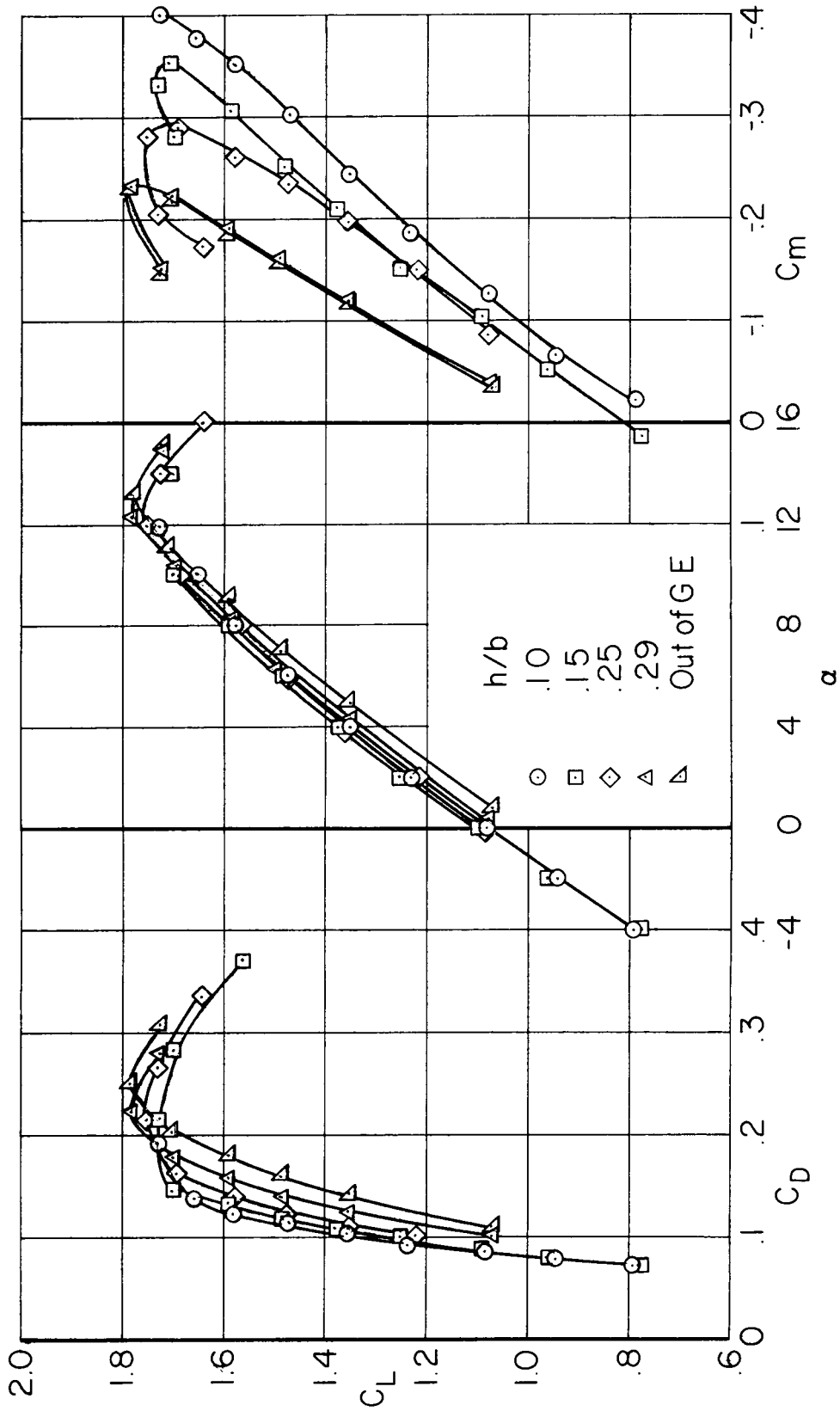
(b) $\delta_f = 30°$, $c_{\mu_{te}} = 0.015$

Figure 6.– Continued.
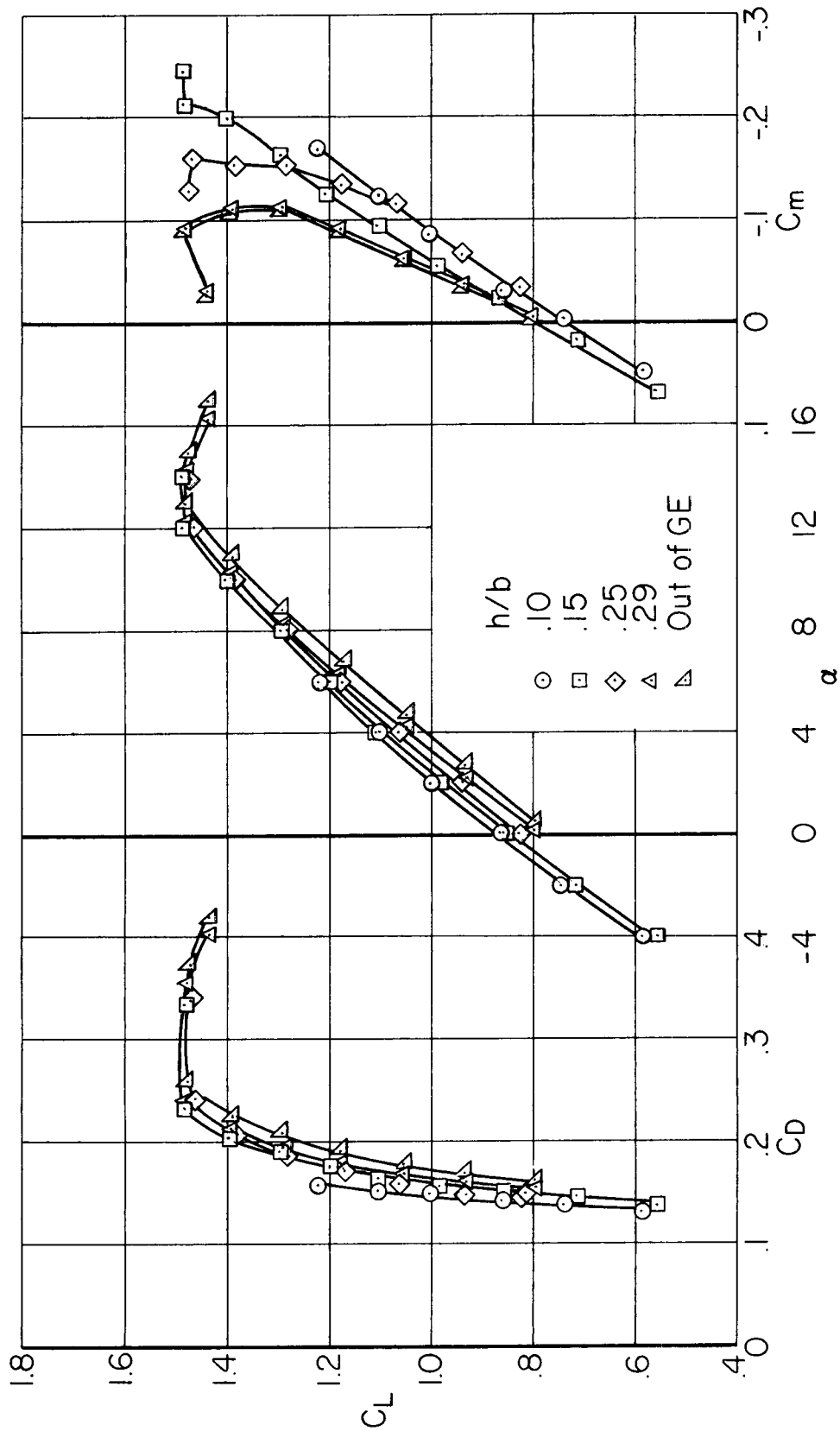
(c) $\delta_f = 50°$, $C_{\mu_{te}} = 0$

Figure 6.- Continued.
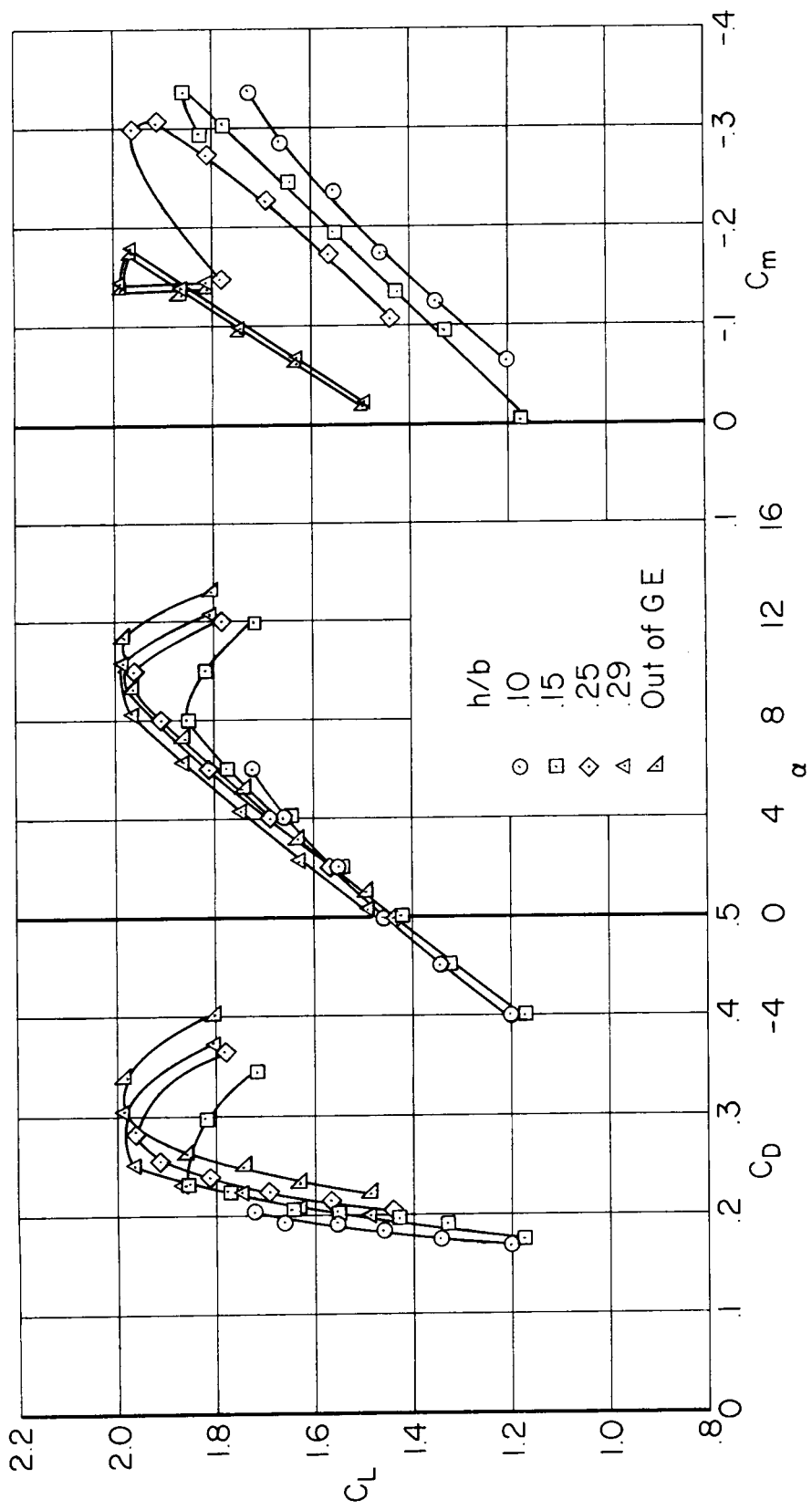
(a) $\delta_f = 50°$, $c_{\mu_{te}} = 0.026$

Figure 6.- Concluded.
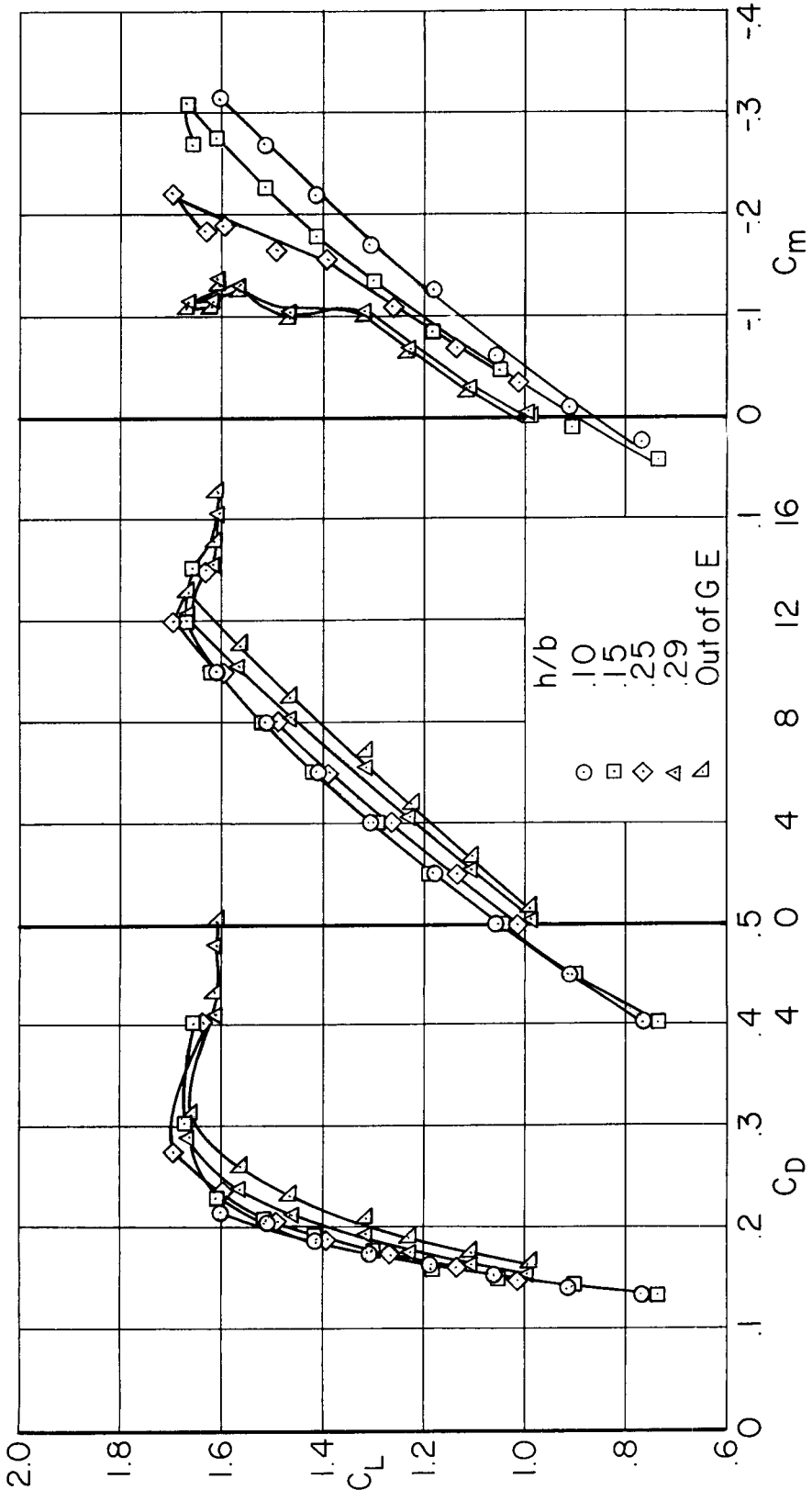
Figure 7.- Effect of ground proximity on the longitudinal characteristics of the model; continuous-span extended chord trailing-edge flap, nacelles and pylons off, $\delta_n = 0^{\circ}$.
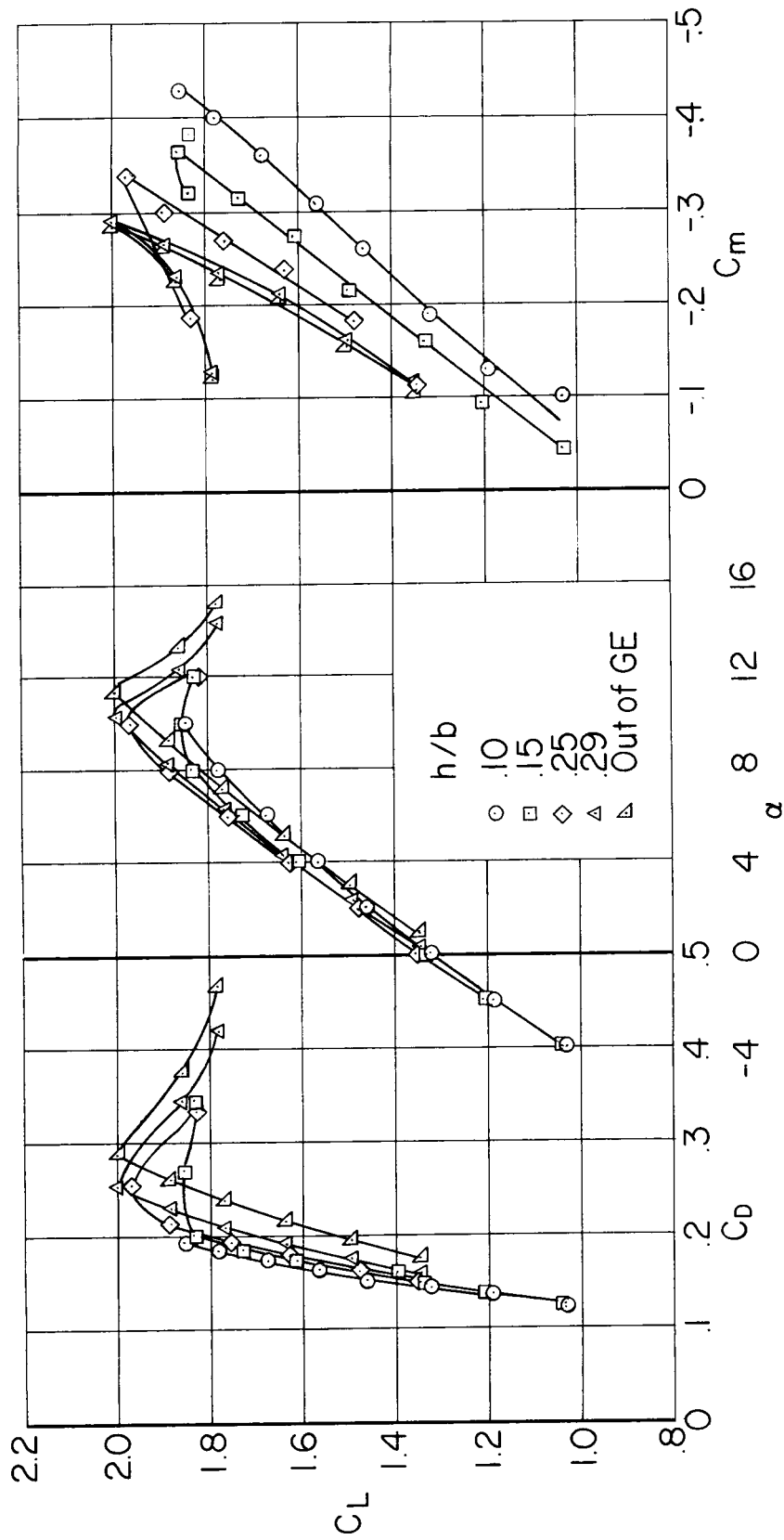
(a) $\delta_f = 30^{\circ}$, $C_{\mu_{te}} = 0$

(b) $\delta_f = 30°$, $C_{\mu_{te}} = 0.017$

Figure 7.- Continued.
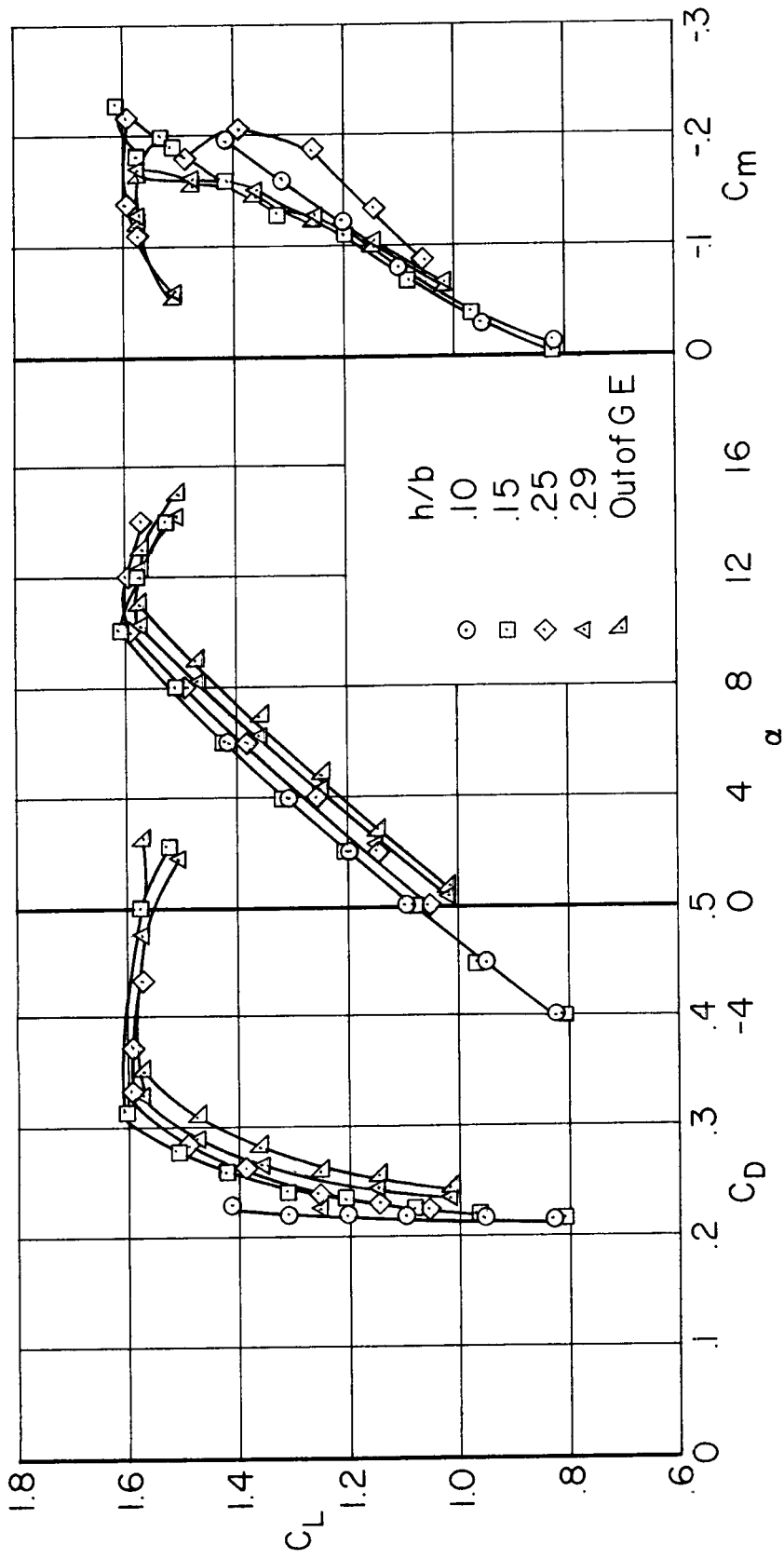
(c) $\delta_f = 50°$, $c_{\mu_{te}} = 0$

Figure 7.- Continued.
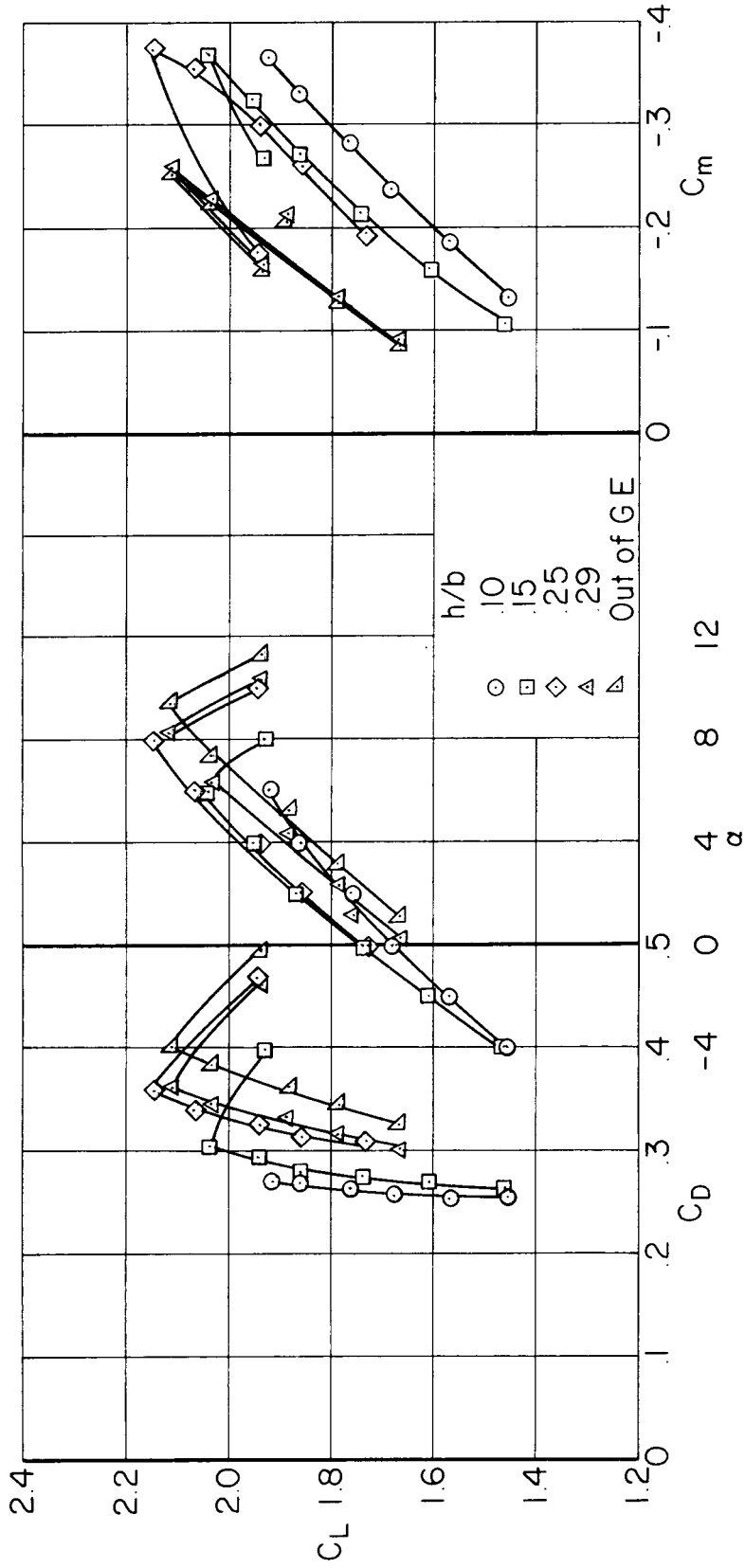
(d) $\delta_f = 50^\circ$, $c_{\mu_{te}} = 0.030$

Figure 7.- Concluded.
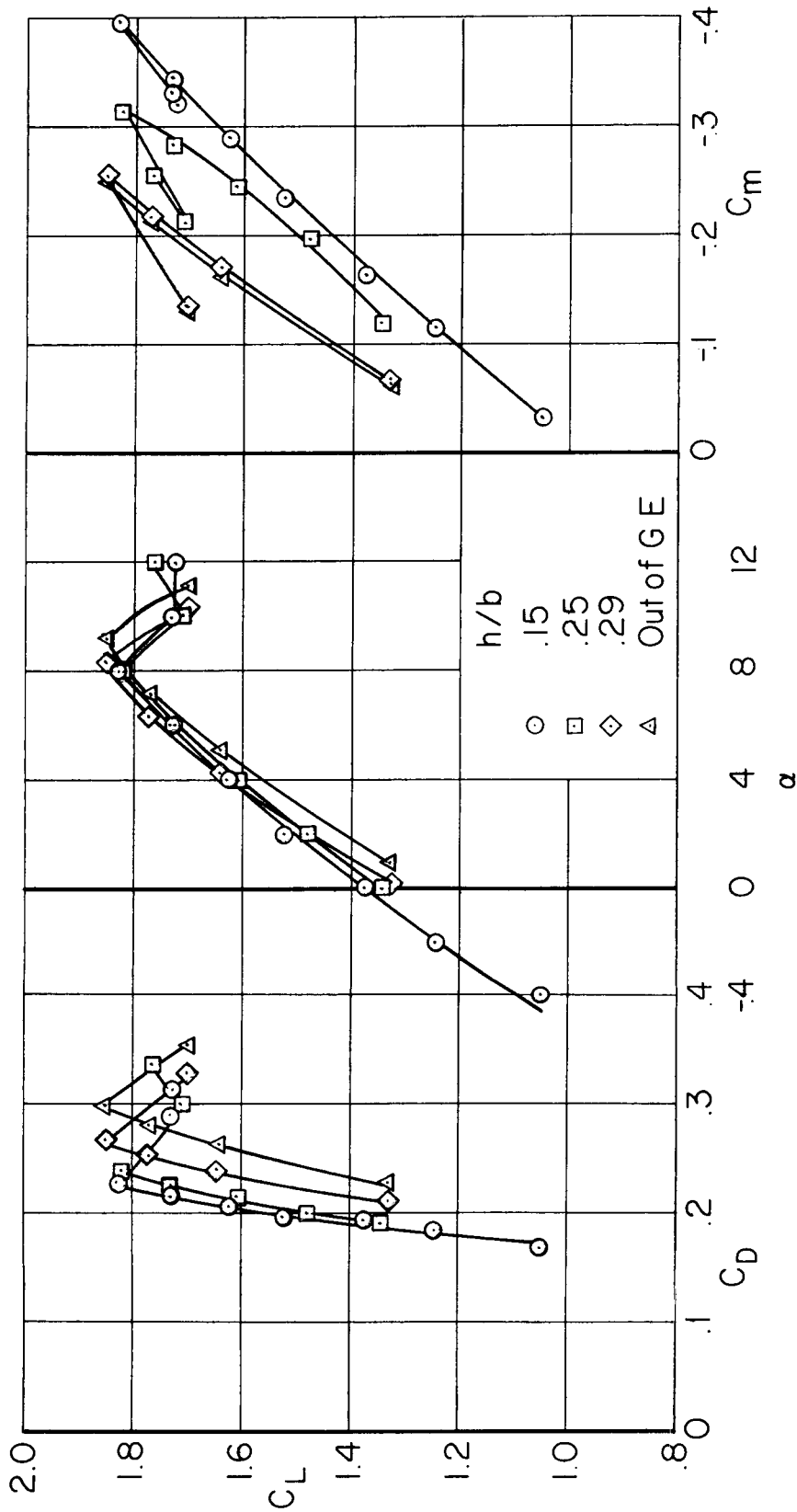
Figure 8.- Effect of ground proximity on the longitudinal characteristics of the model; leading-edge flap deflected 50°, continuous-span normal trailing-edge flap deflected 50°, $C_{\mu_{te}} = 0.025$, nacelles and pylons off.

(a) $C_{\mu_{le}} = 0$

31
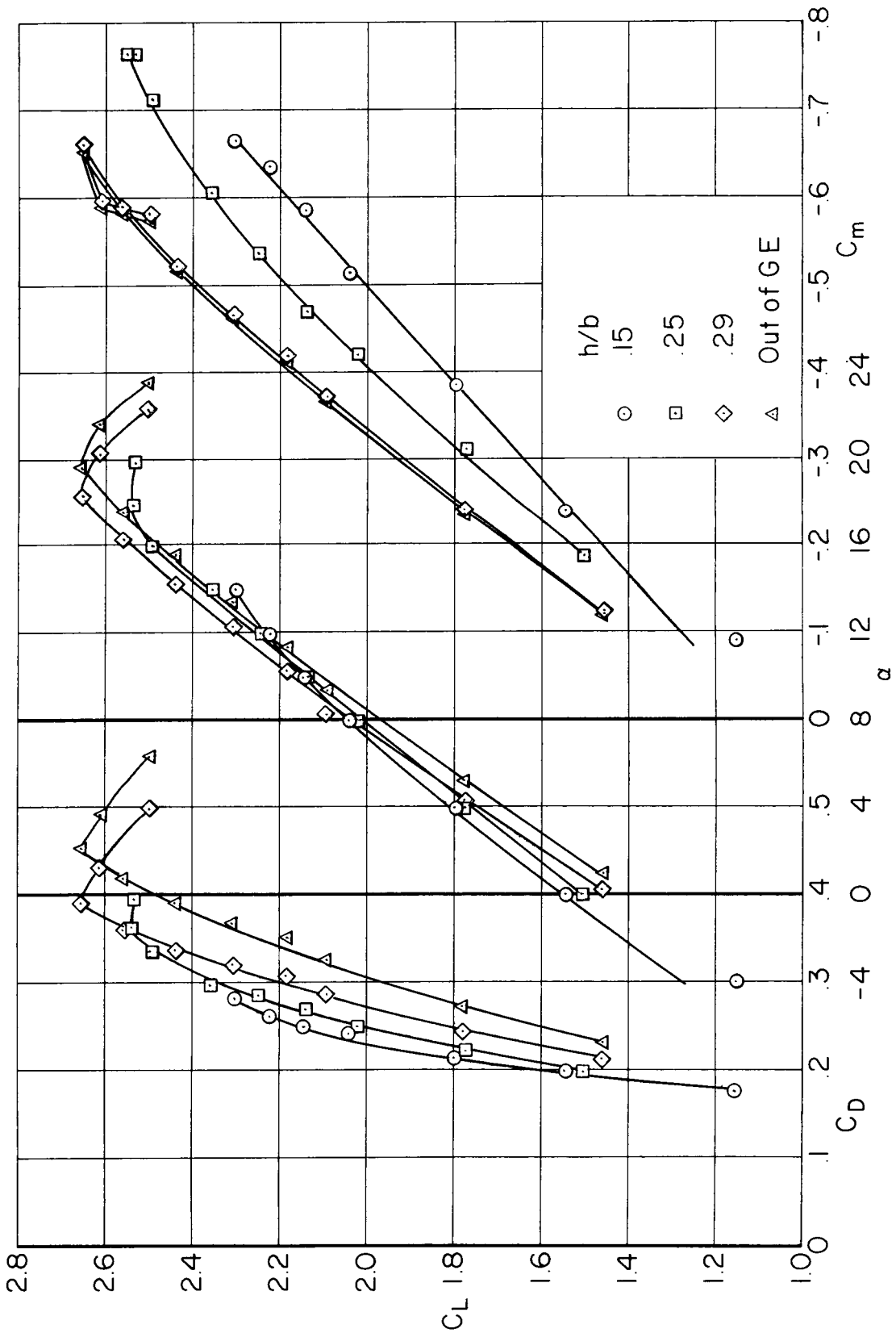
(b) $C_{\mu_{le}} = 0.041$

Figure 8.- Concluded.
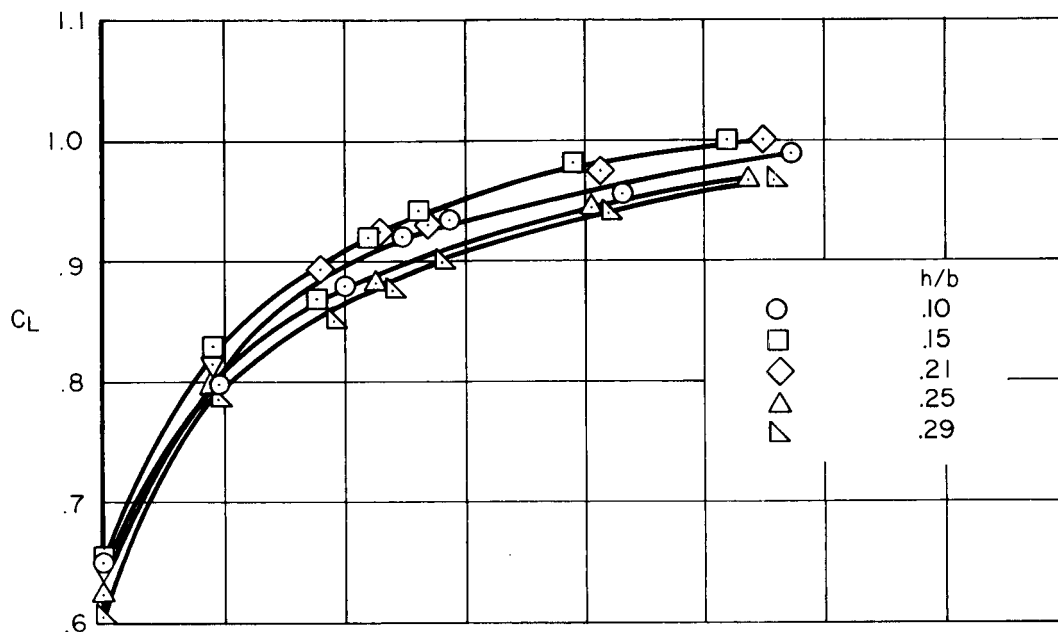
(a) Normal flap, $\delta_f = 30^\circ$.
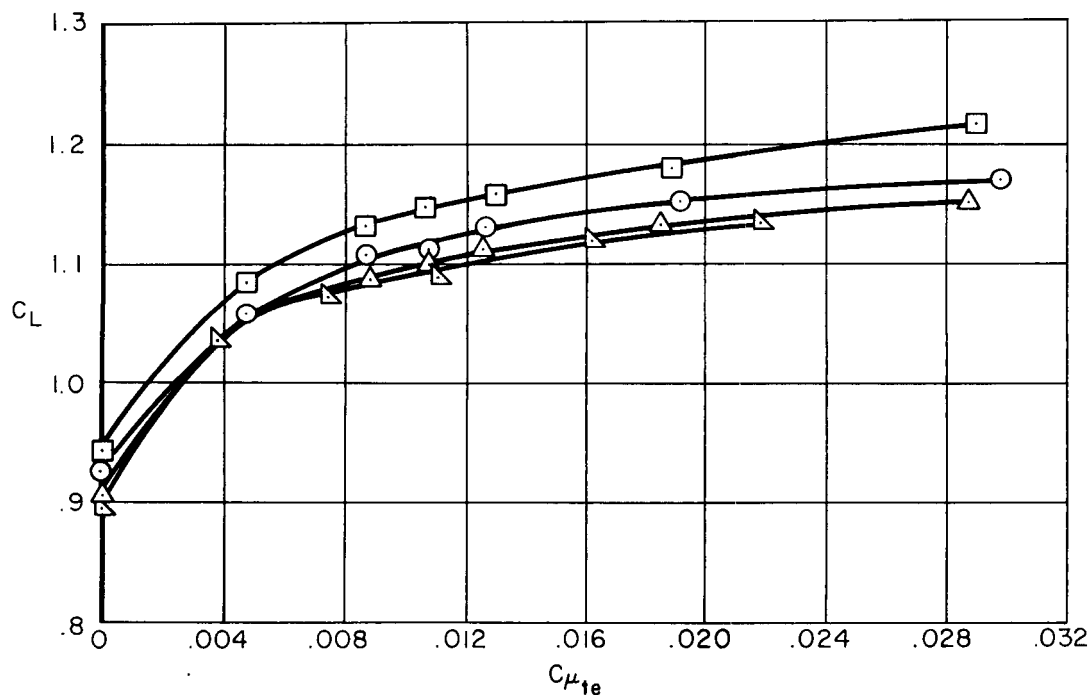
(b) Extended chord flap, $\delta_f = 30^\circ$

Figure 9.- Effect of ground proximity on the variation of lift coefficient with momentum coefficient; interrupted-span trailing-edge flap, nacelles and pylons on, $\delta_n = 0^\circ$, $\alpha = 0^\circ$.
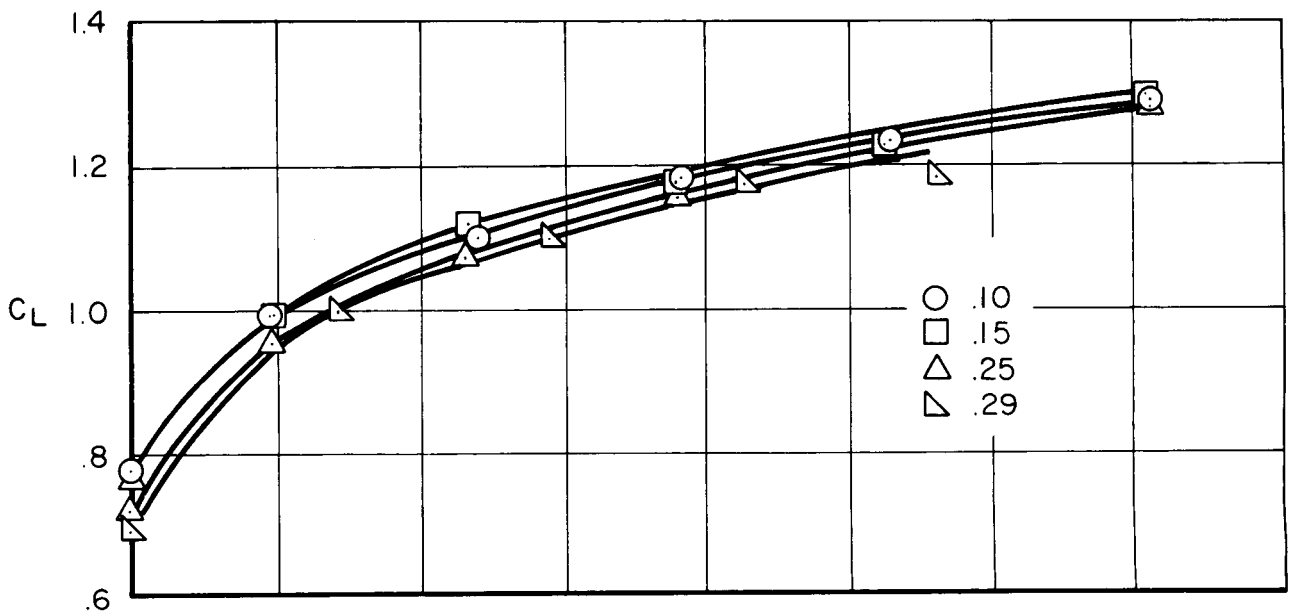
(c) Normal flap, $\delta_f = 50^\circ$.
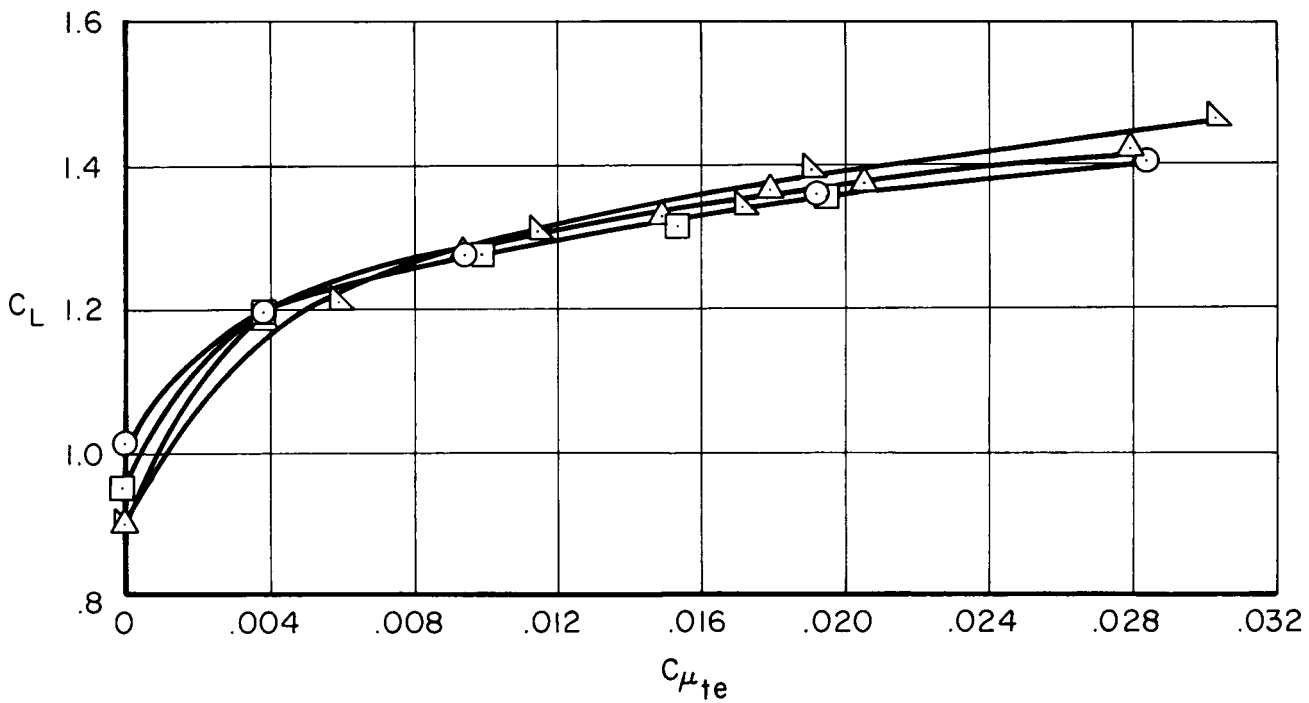
(d) Extended chord flap, $\delta_f = 50^\circ$

Figure 9.- Concluded.

(a) Normal flap, $\delta_f = 30^O$.

(b) Extended chord flap, $\delta_f = 30^O$.

Figure 10.- Effect of ground proximity on the variation of lift coefficient with momentum coefficient; continuous-span trailing-edge flap, nacelles and pylons off, $\delta_n = 0^O$, $\alpha = 0^O$.
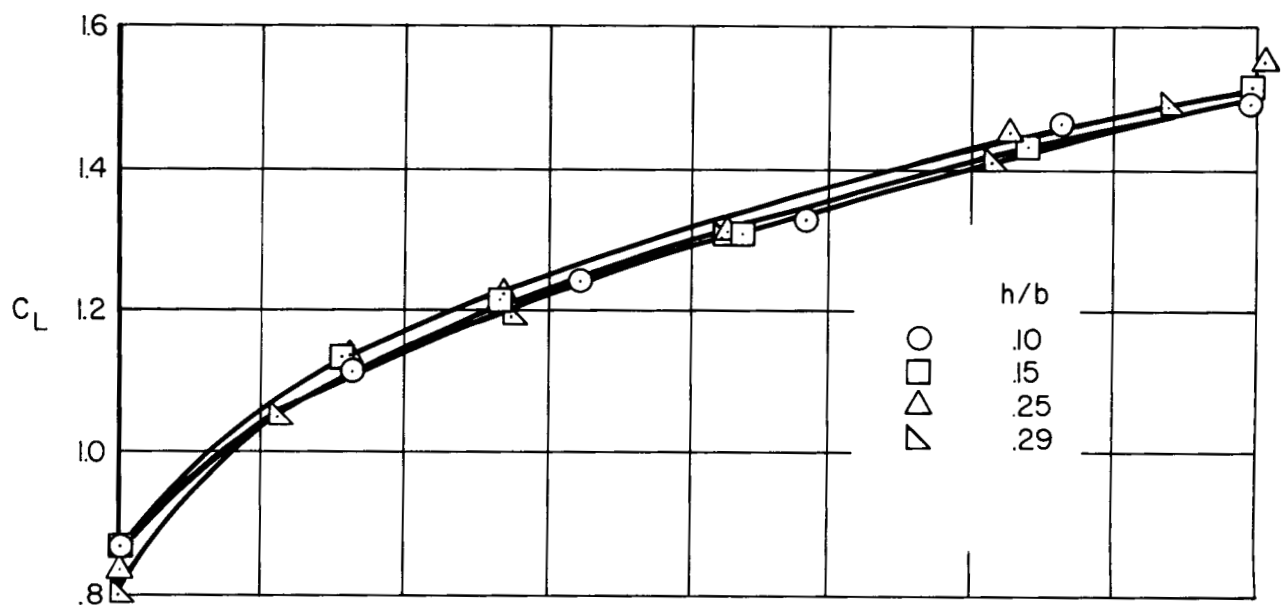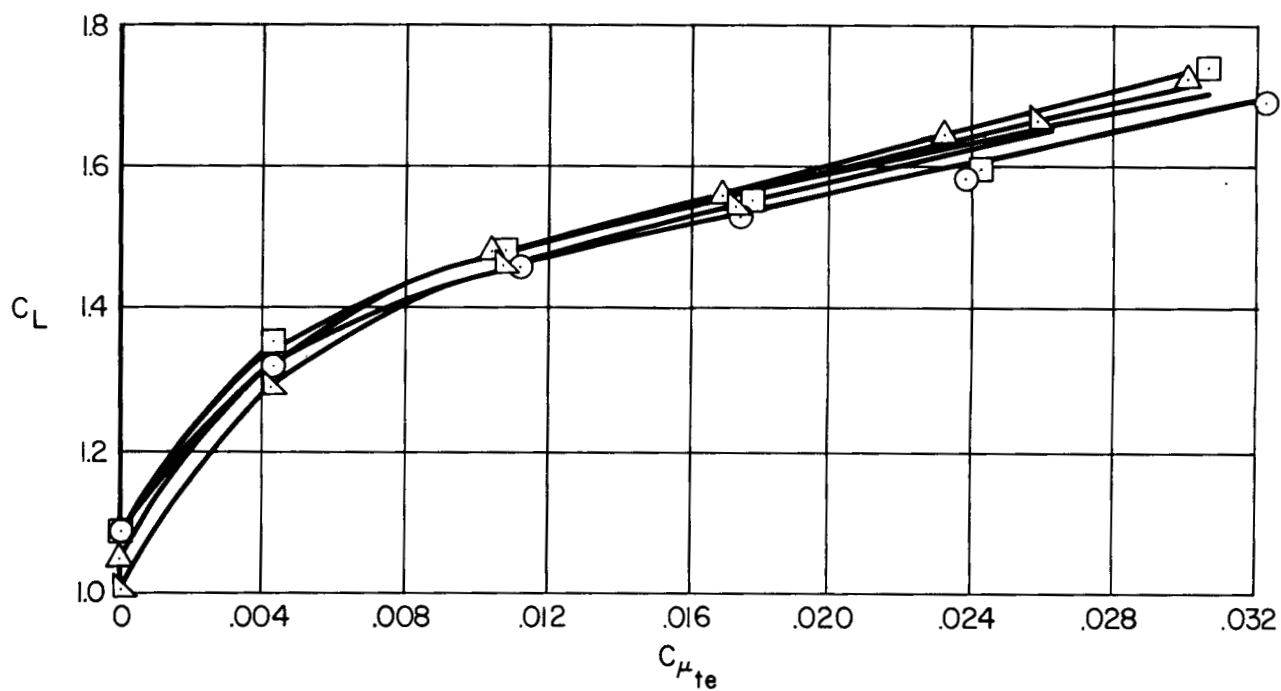
(c) Normal flap, $\delta_f = 50^\circ$.

(d) Extended chord flap, $\delta_f = 50^\circ$.

Figure 10.- Concluded.
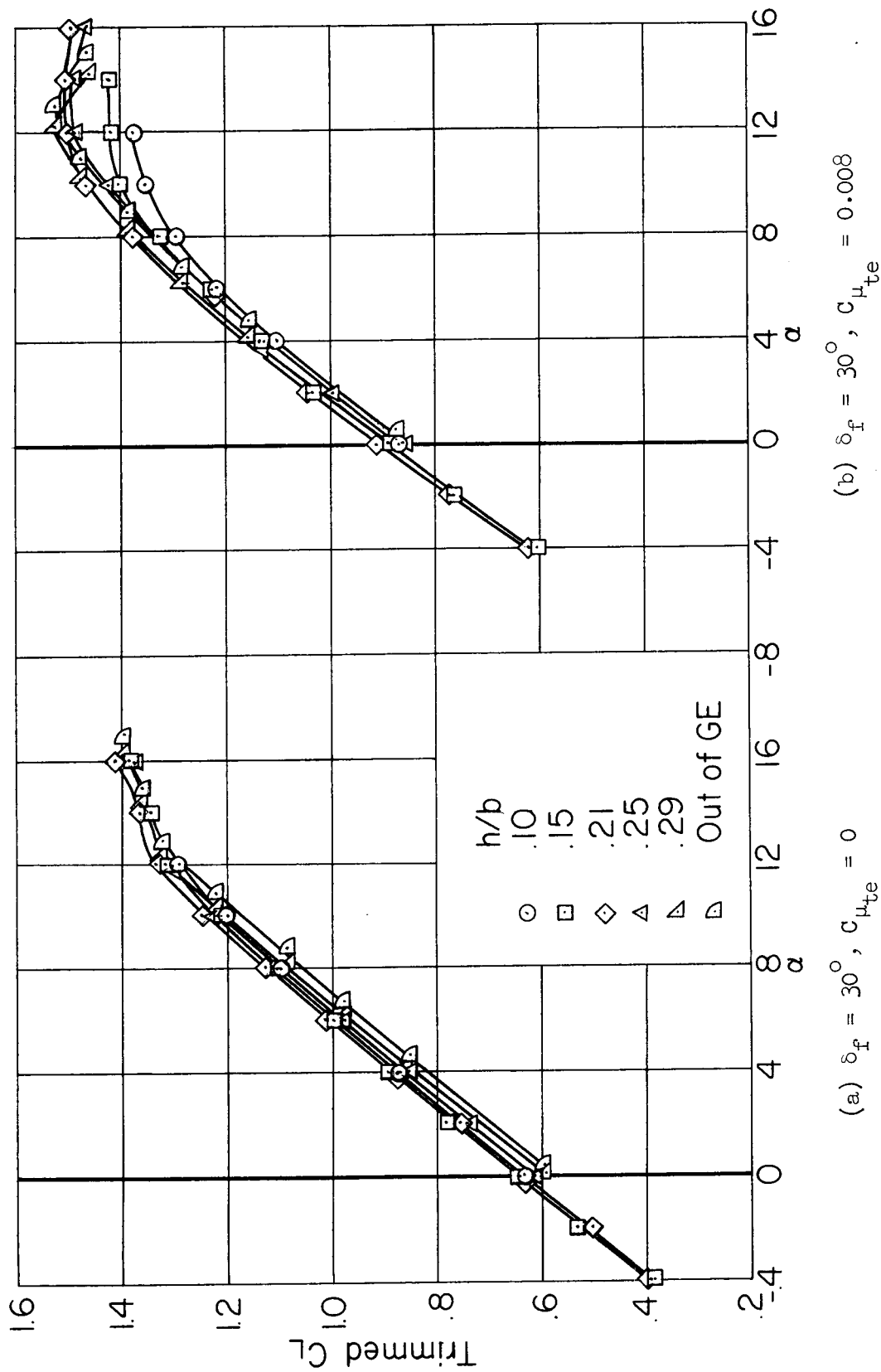
Figure 11.- Effect of ground proximity on the trimmed lift coefficient of the model; interrupted-span normal trailing-edge flap, nacelles and pylons on, $\delta_n = 0^\circ$.
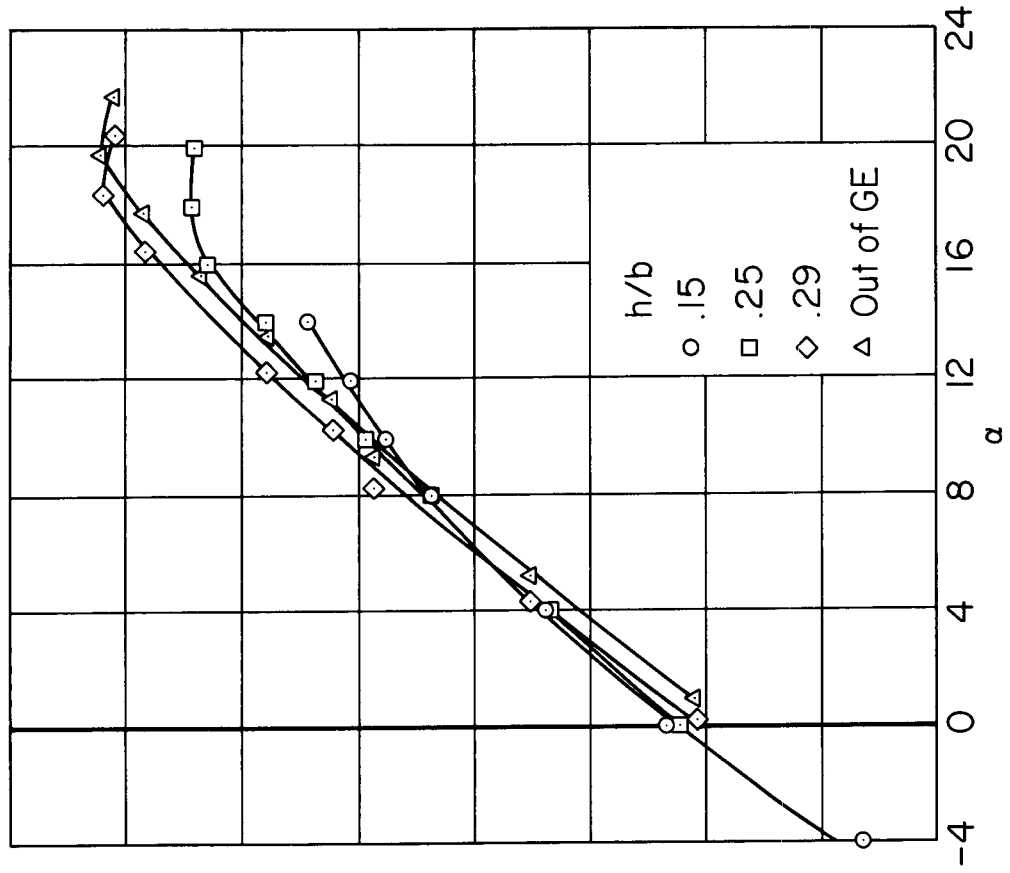
(a) $\delta_f = 30^\circ$, $c_{\mu_{te}} = 0$
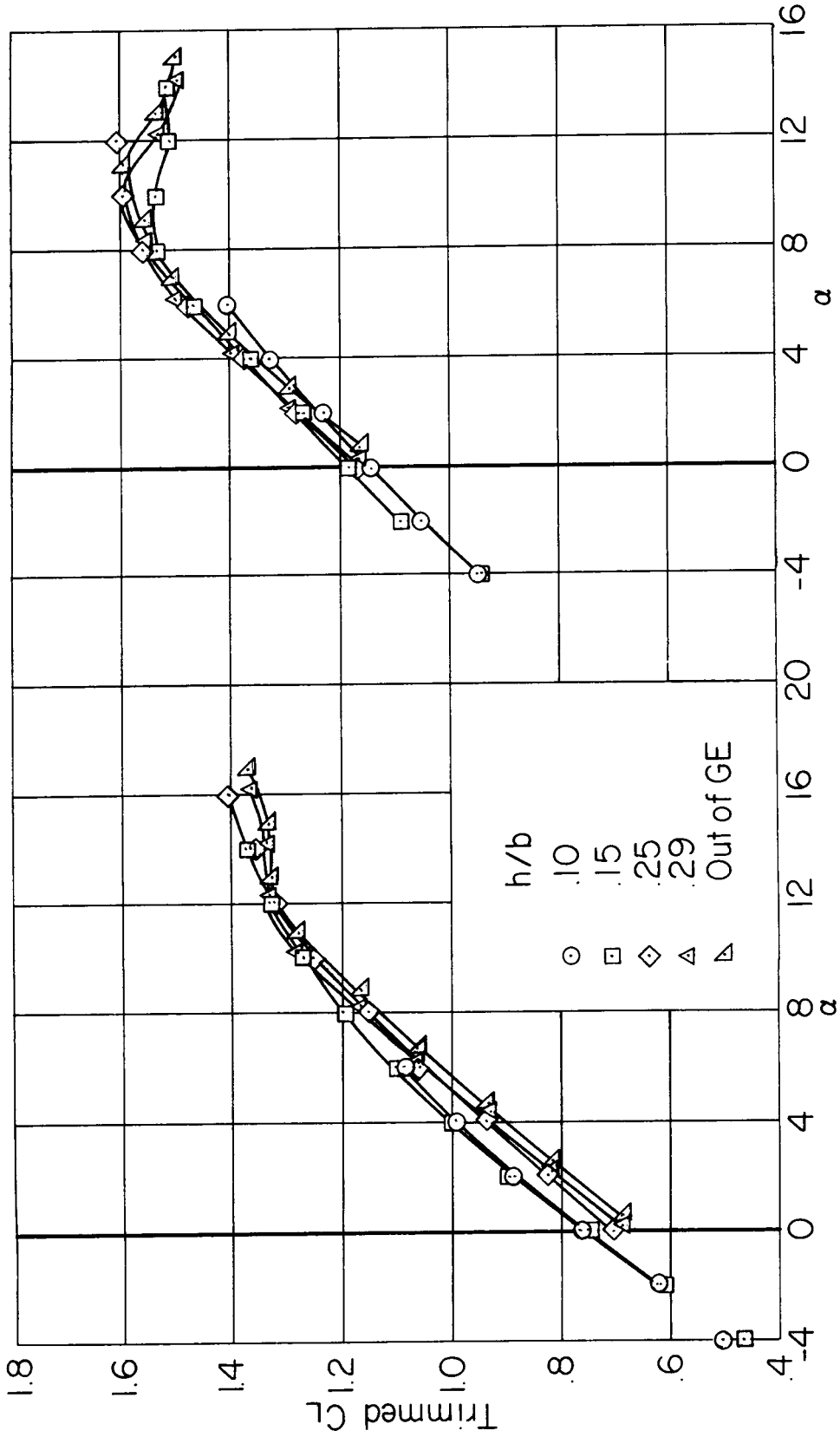
(b) $\delta_f = 30^\circ$, $c_{\mu_{te}} = 0.008$

(c) $\delta_f = 50°$, $C_{\mu_{te}} = 0$

(d) $\delta_f = 50°$, $C_{\mu_{te}} = 0.015$

Figure 11.- Concluded.

Figure 12.- Effect of ground proximity on the trimmed lift coefficient of the model; interrupted-span extended chord trailing-edge flap, nacelles and pylons on, $\delta_n = 0^\circ$.

(a) $\delta_f = 30^\circ$, $c_{\mu_{te}} = 0$

(b) $\delta_f = 30^\circ$, $c_{\mu_{te}} = 0.010$
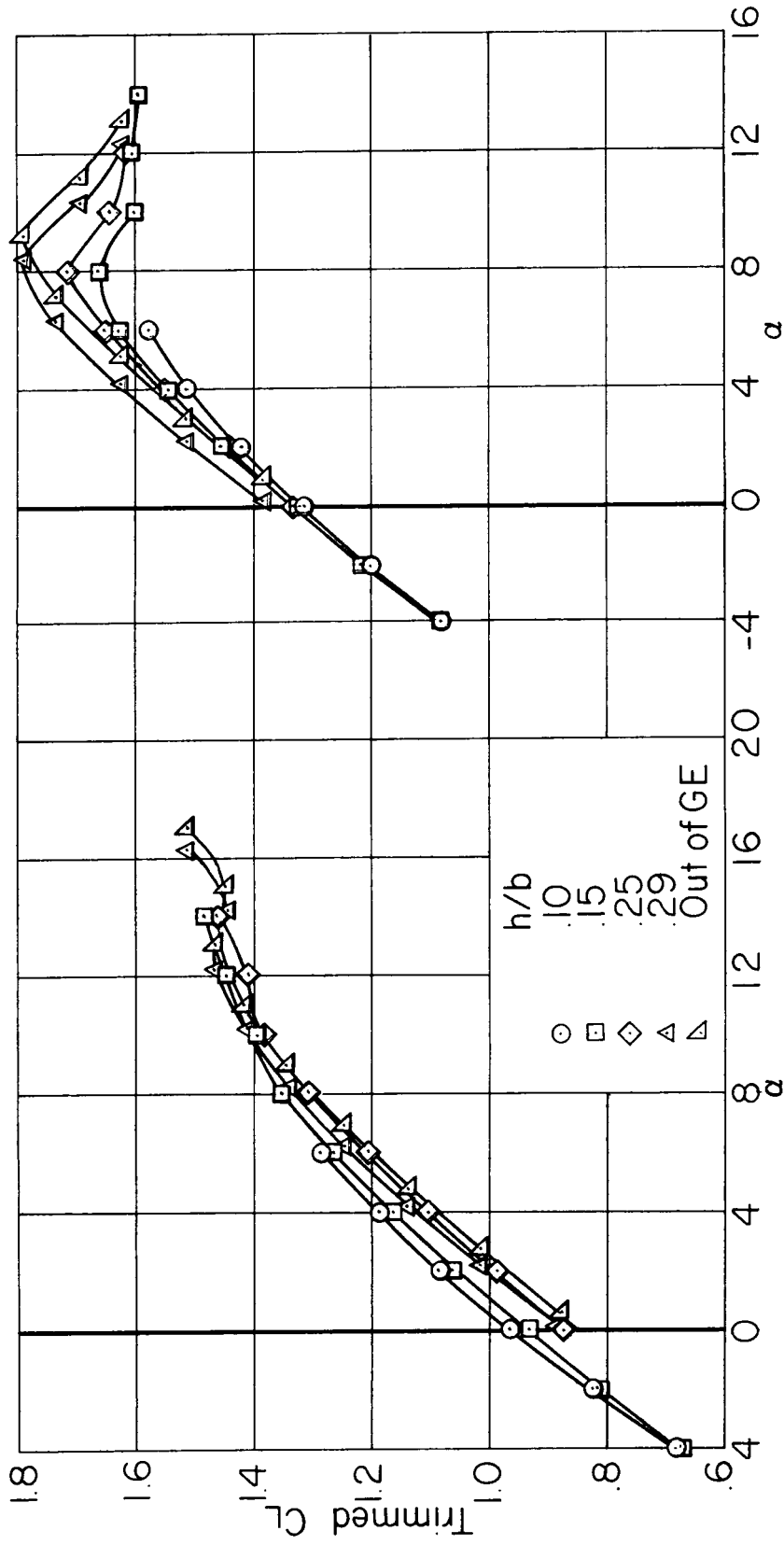
(c) $\delta_f = 50°$, $c_{\mu_{te}} = 0$ (d) $\delta_f = 50°$, $c_{\mu_{te}} = 0.019$

Figure 12.- Concluded.

(a) $\delta_f = 30°$, $C\mu_{te} = 0$ (b) $\delta_f = 30°$, $C\mu_{te} = 0.015$
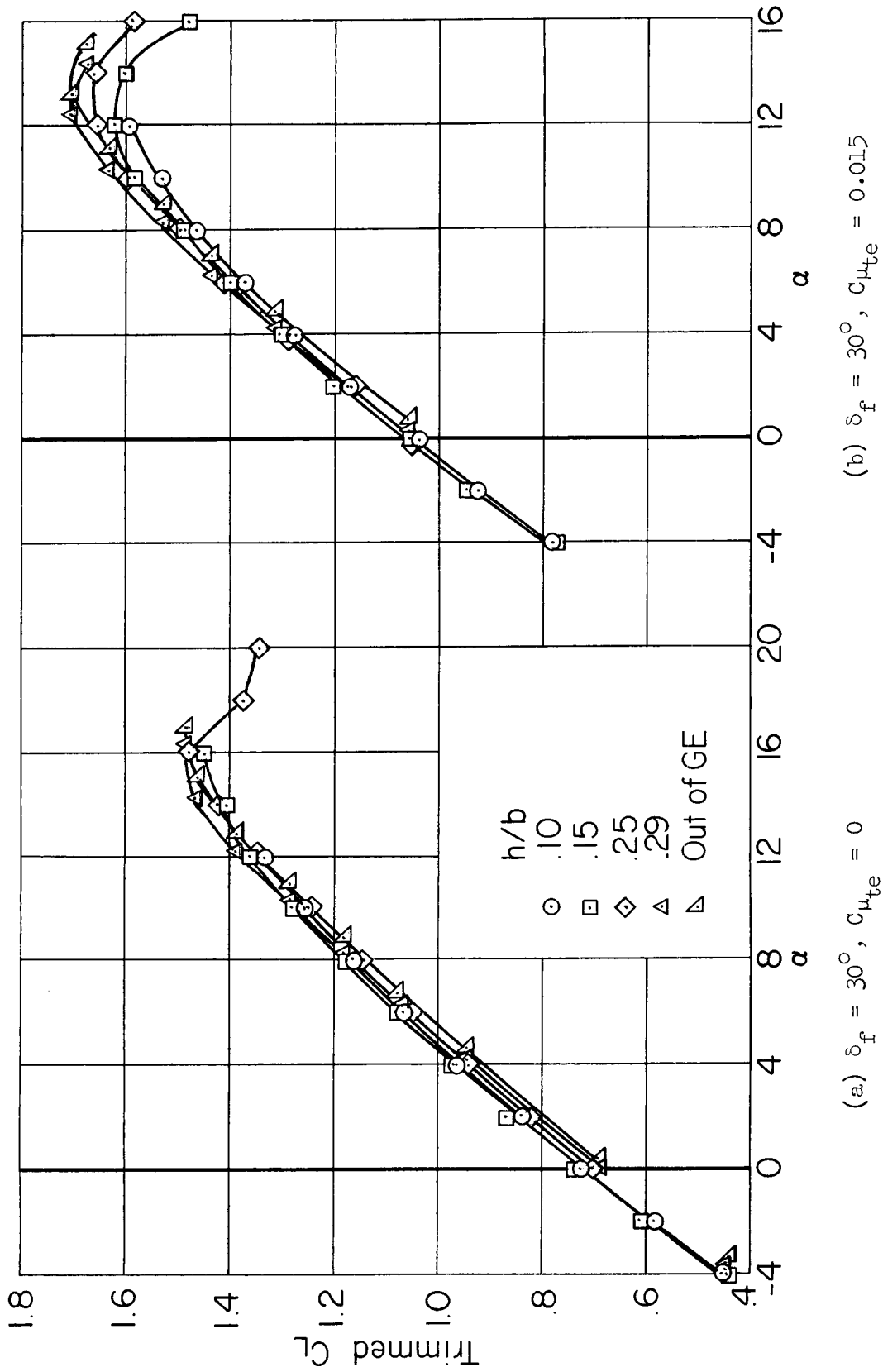
Figure 13.- Effect of ground proximity on the trimmed lift coefficient of the model; continuous-span normal trailing-edge flap, nacelles and pylons off, $\delta_n = 0°$.
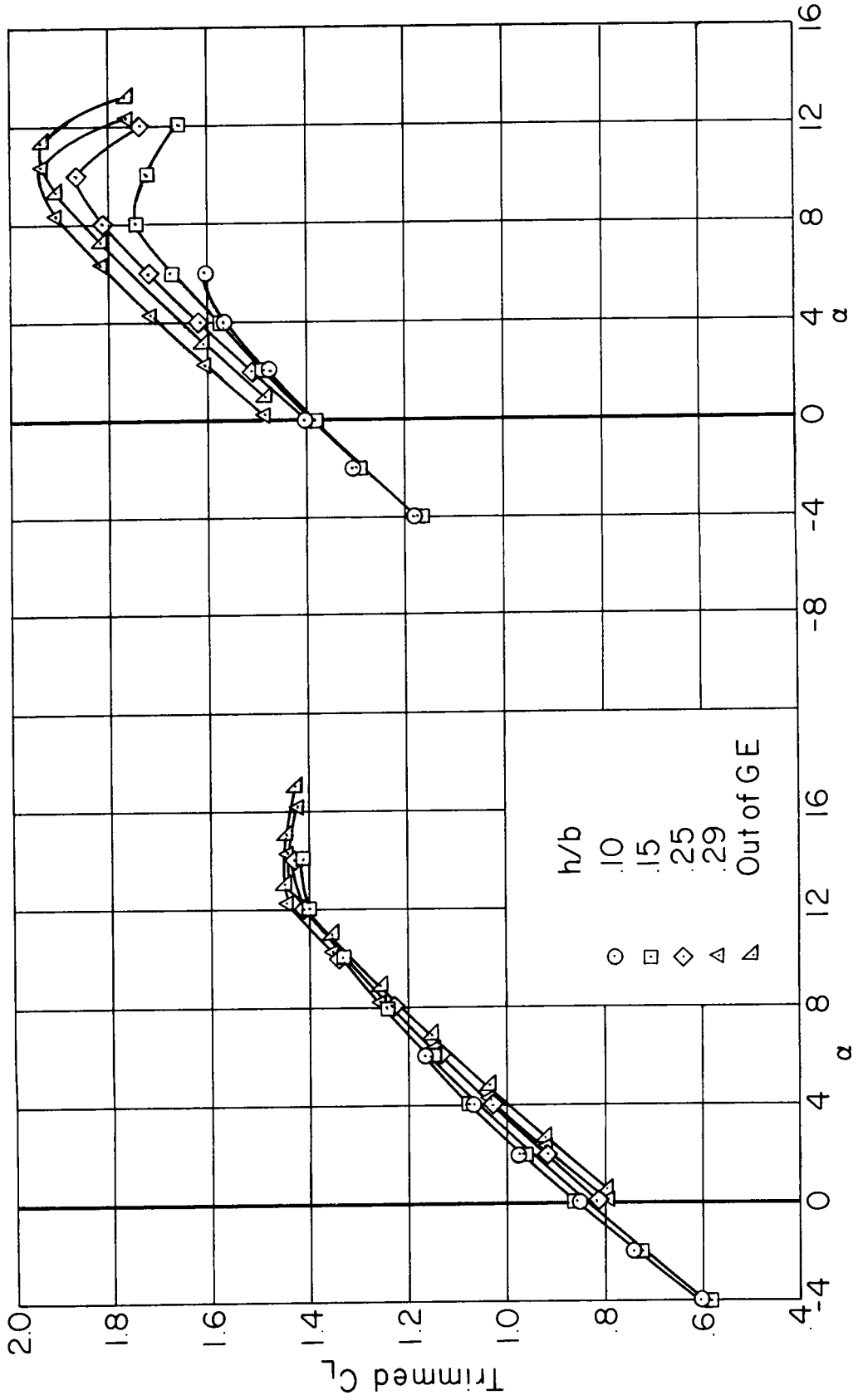
(c) $\delta_f = 50°$, $c_{\mu_{te}} = 0$

(d) $\delta_f = 50°$, $c_{\mu_{te}} = 0.026$

Figure 13.- Concluded.
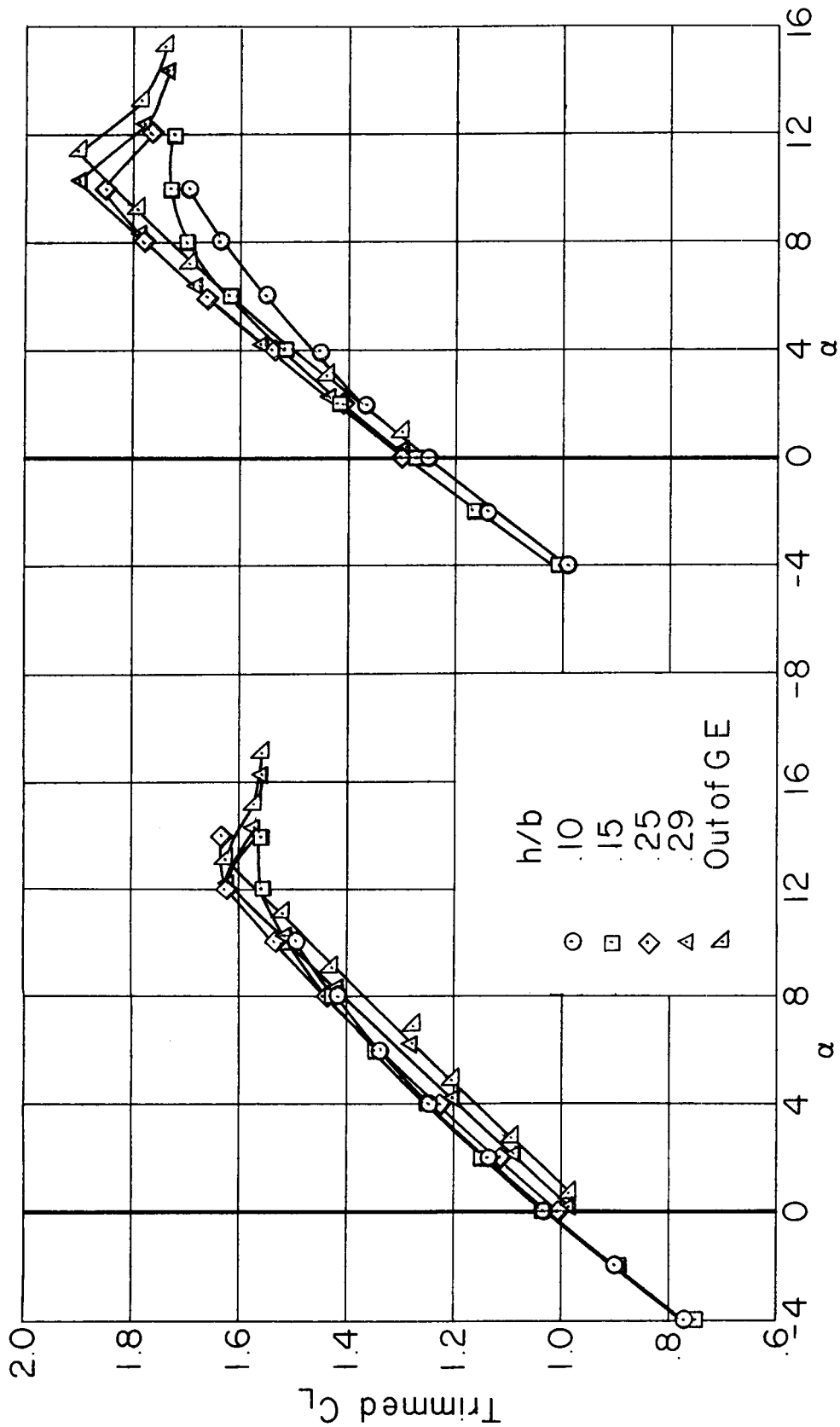
Figure 14.- Effect of ground proximity on the trimmed lift coefficient of the model; continuous-span extended chord trailing-edge flap, nacelles and pylons on, $\delta_n = 0^\circ$.

(a) $\delta_f = 30^\circ$, $C_{\mu_{te}} = 0$

(b) $\delta_f = 30^\circ$, $C_{\mu_{te}} = 0.017$
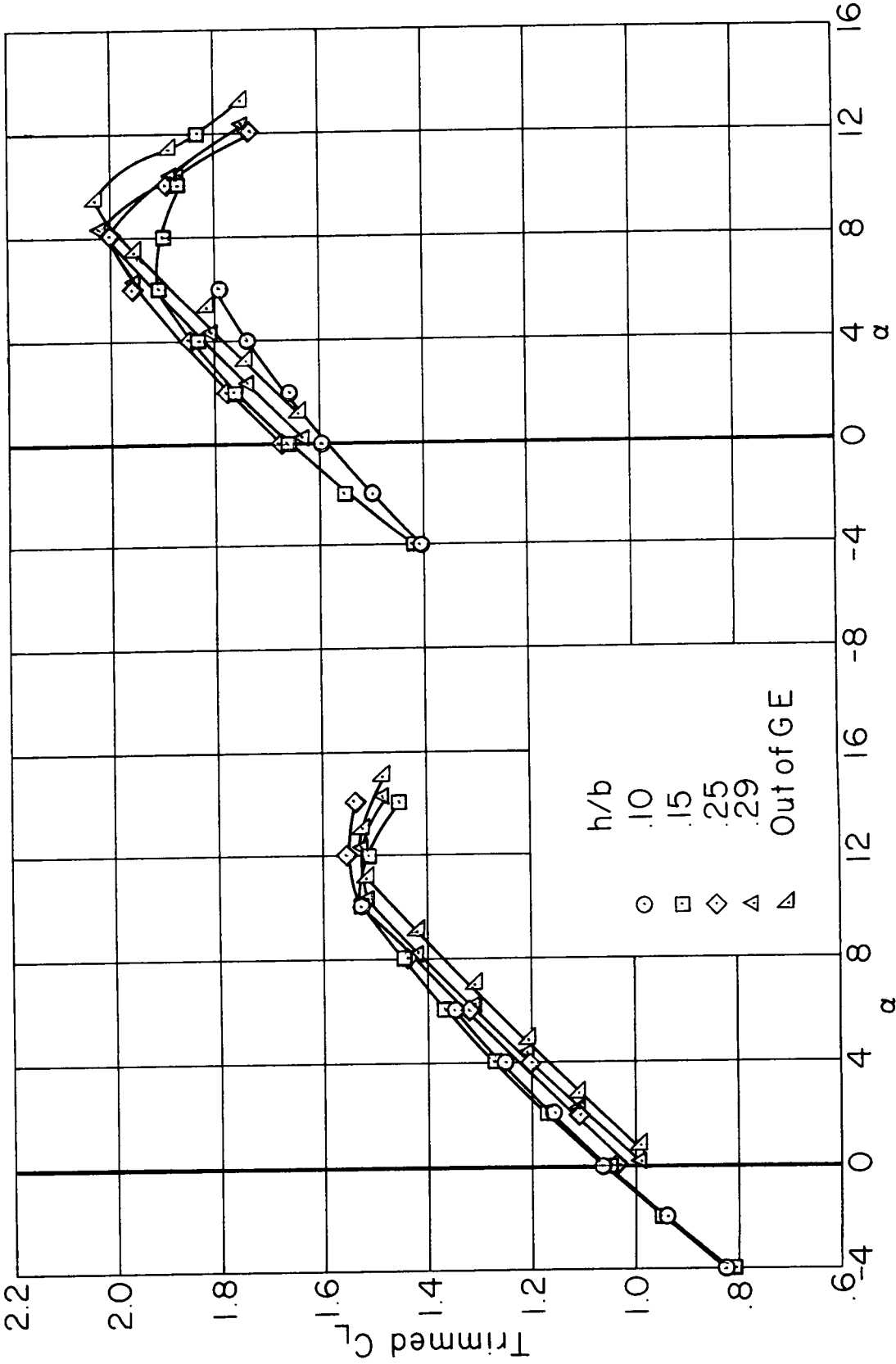
(c) $\delta_f = 50^\circ$, $c_{\mu_{te}} = 0$

(d) $\delta_f = 50^\circ$, $c_{\mu_{te}} = 0.030$

Figure 14.- Concluded.
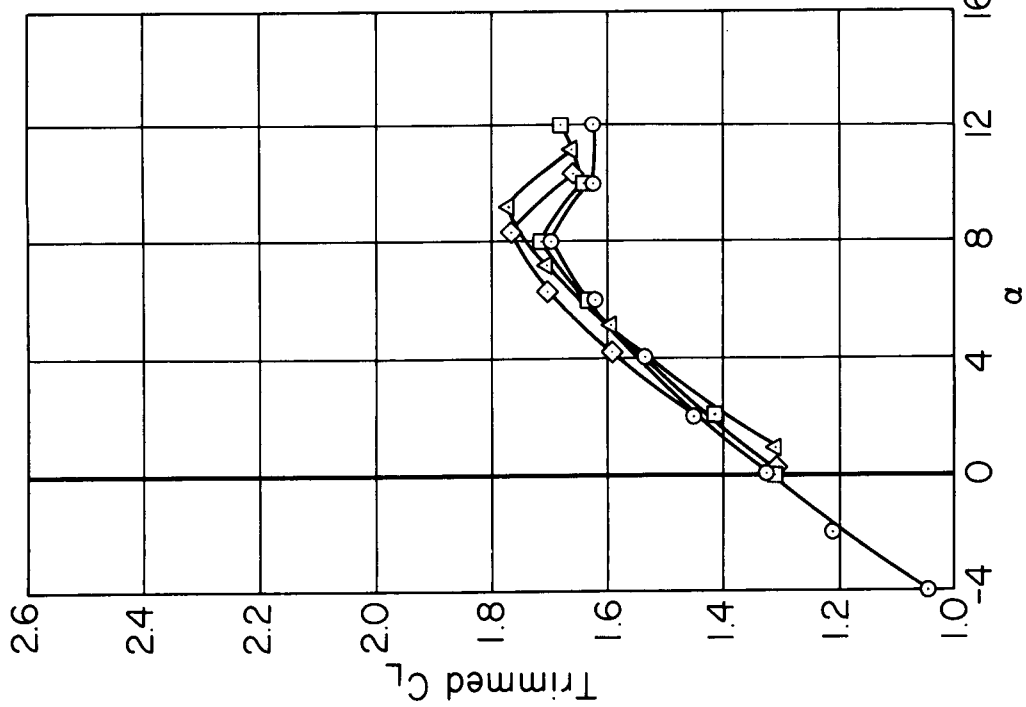
Figure 15.- Effect of ground proximity on the trimmed lift coefficient of the model; leading-edge flap deflected 50°, continuous-span normal trailing-edge flap deflected 50°, $C_{\mu_{te}} = 0.025$, nacelles and pylons off.

(a) $C_{\mu_{le}} = 0$

(b) $C_{\mu_{le}} = 0.041$
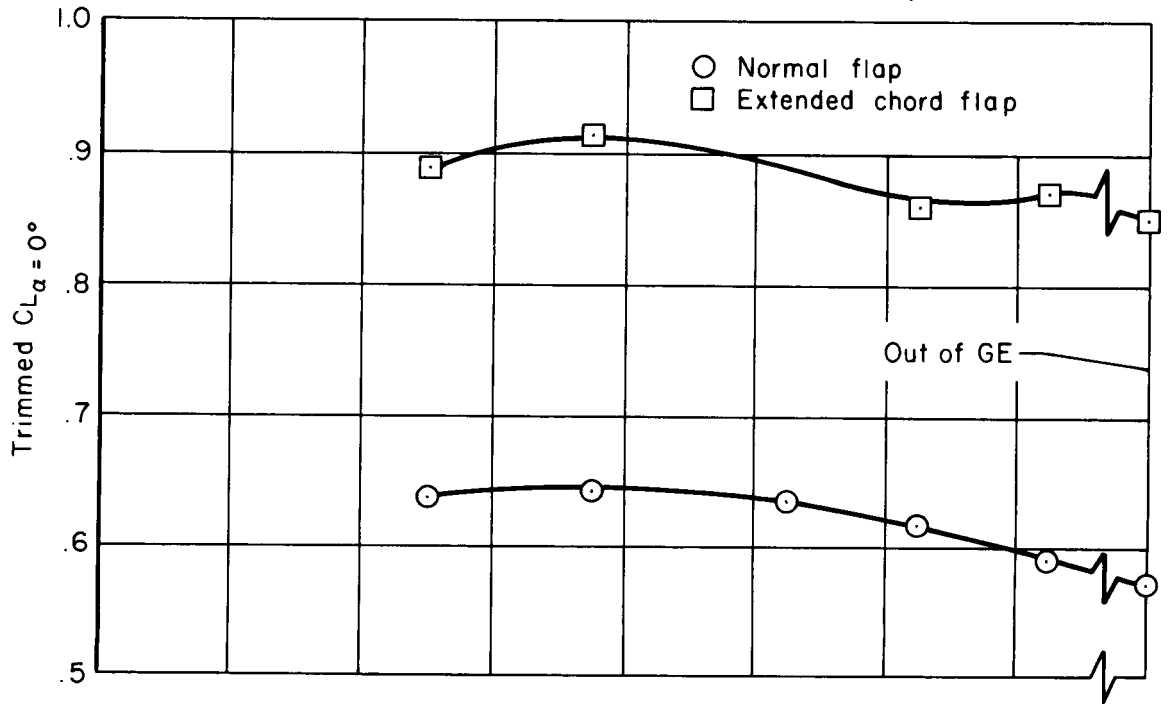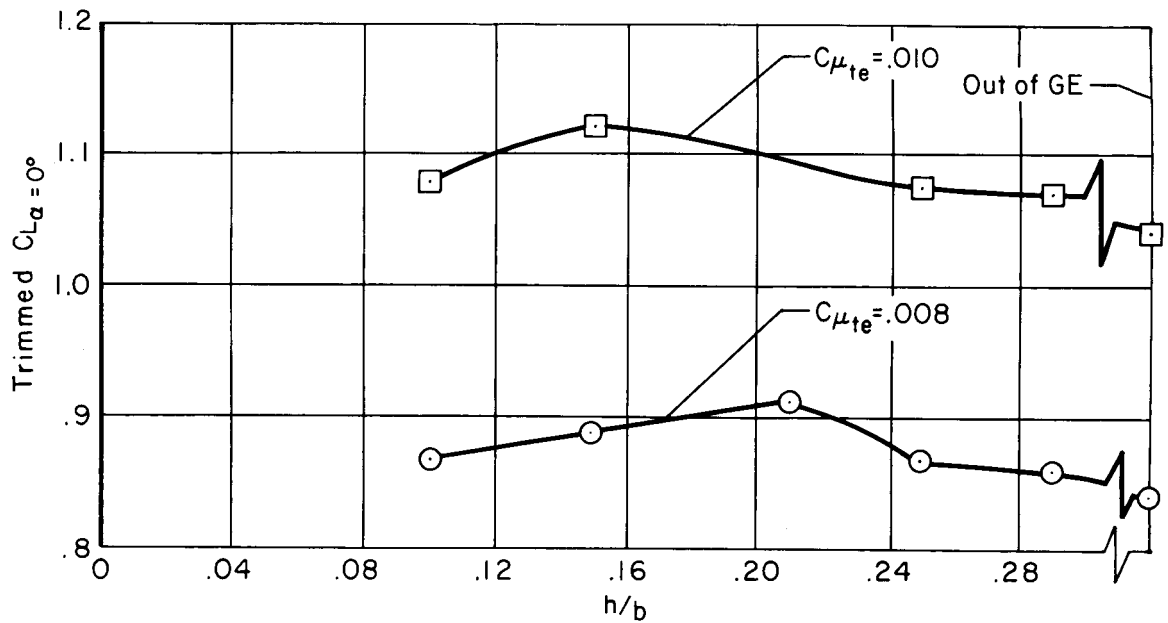
(a) $\delta_f = 30^\circ$ without BLC.

(b) $\delta_f = 30^\circ$ with BLC.

Figure 16.- Variation of trimmed lift coefficient with ground proximity; interrupted-span flap, nacelles and pylons on, $\delta_n = 0^\circ$, $\alpha = 0^\circ$.
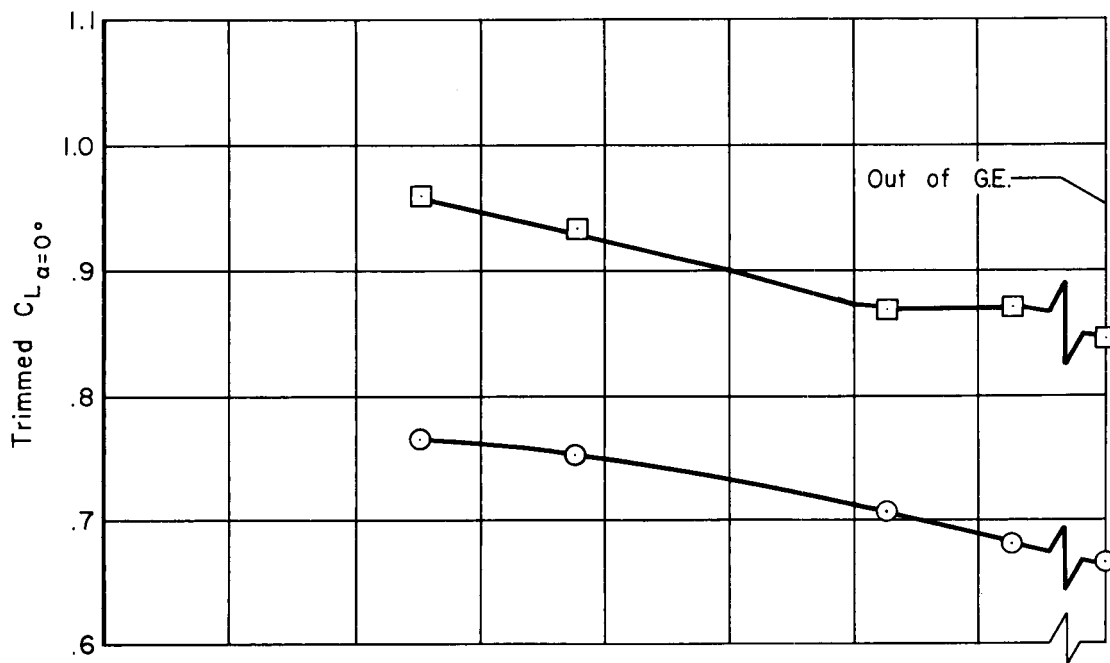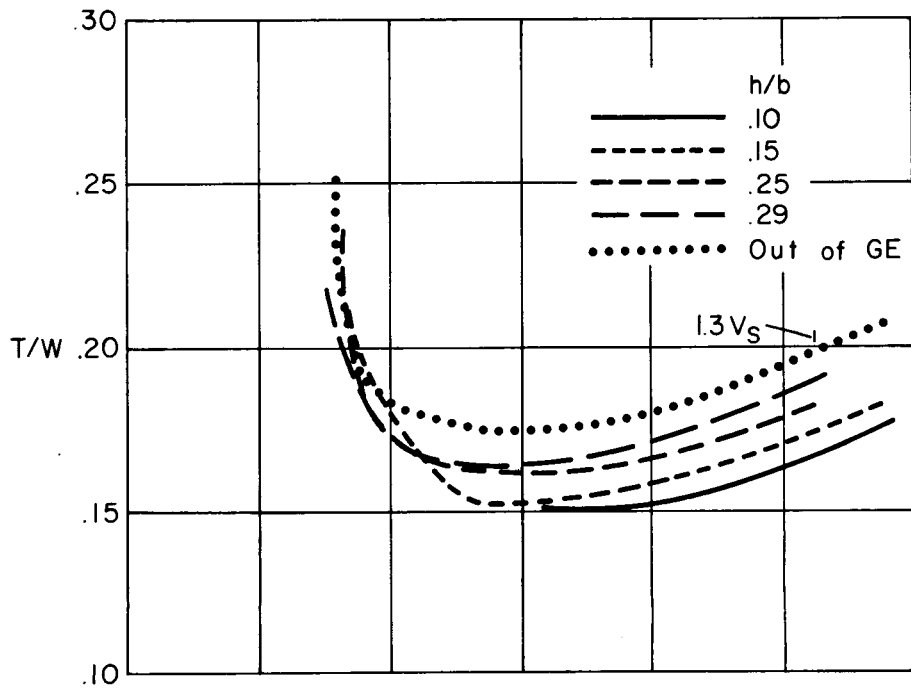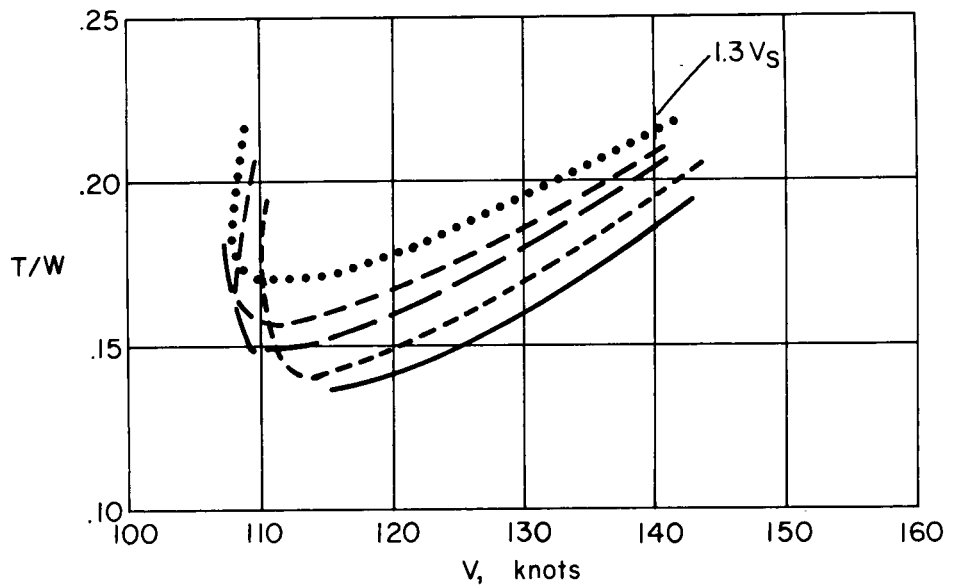
(c) $\delta_f = 50^{\circ}$ without BLC.
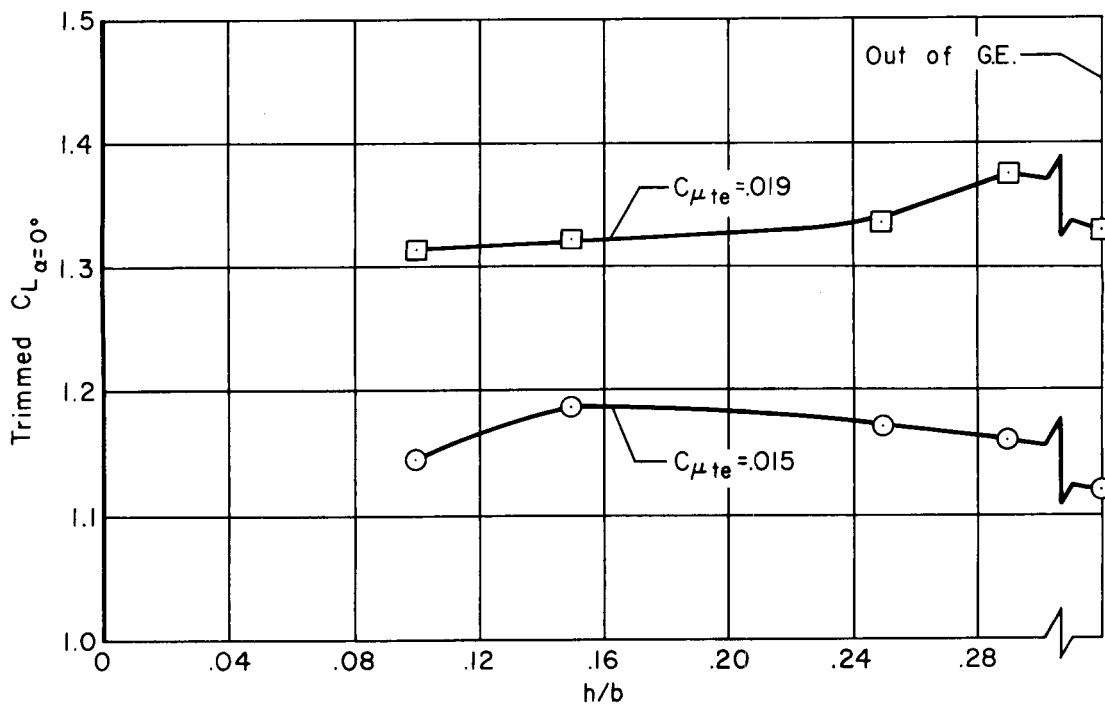
(d) $\delta_f = 50^{\circ}$ with BLC.

Figure 16.- Concluded.
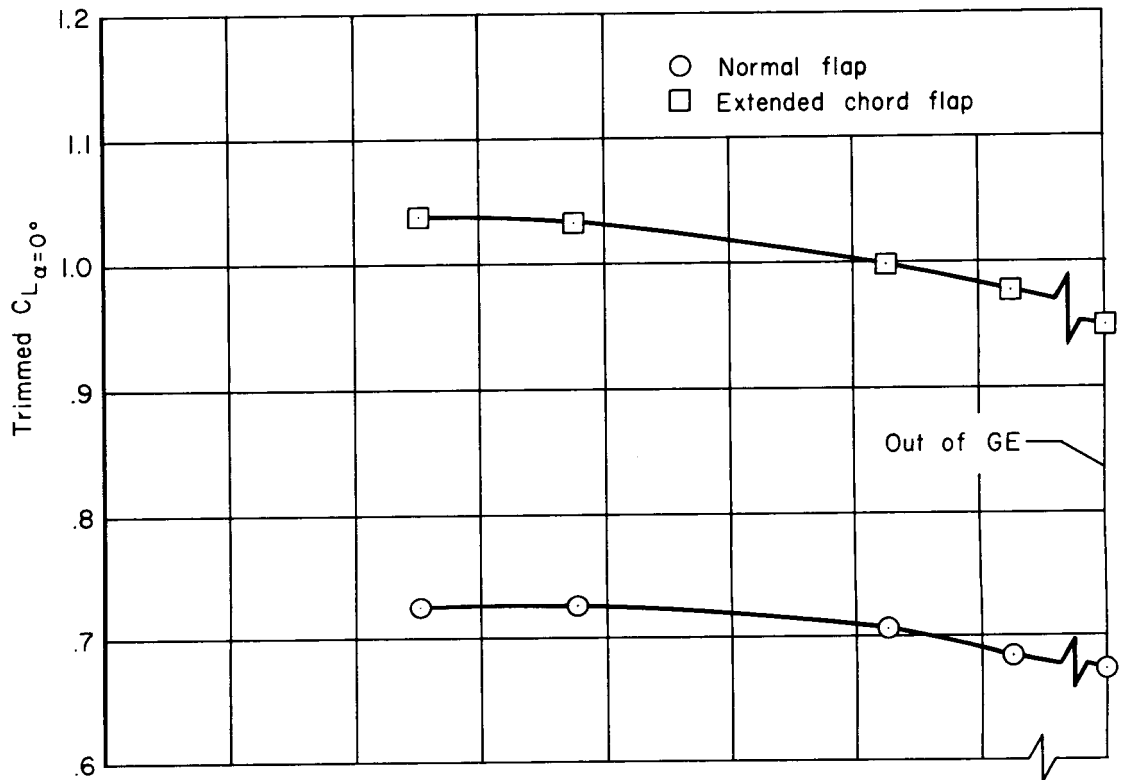
(a) $\delta_f = 30^\circ$ without BLC.
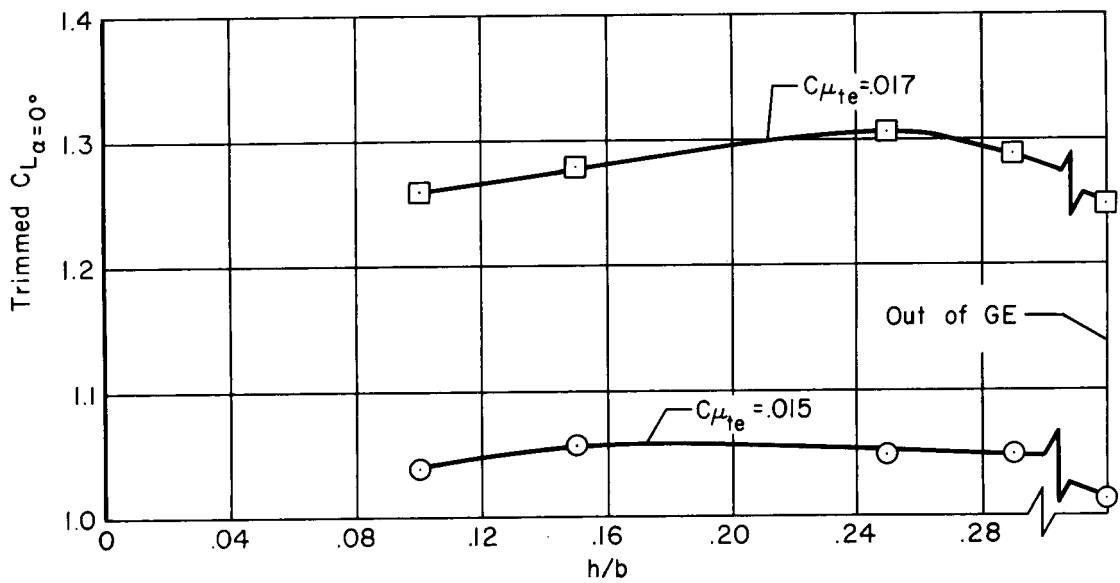
(b) $\delta_f = 30^\circ$ with BLC.

Figure 17.- Variation of trimmed lift coefficient with ground proximity; continuous-span flap, nacelles and pylons off, $\delta_n = 0^\circ$, $\alpha = 0^\circ$.

(c) $\delta_f = 50^{O}$ without BLC.
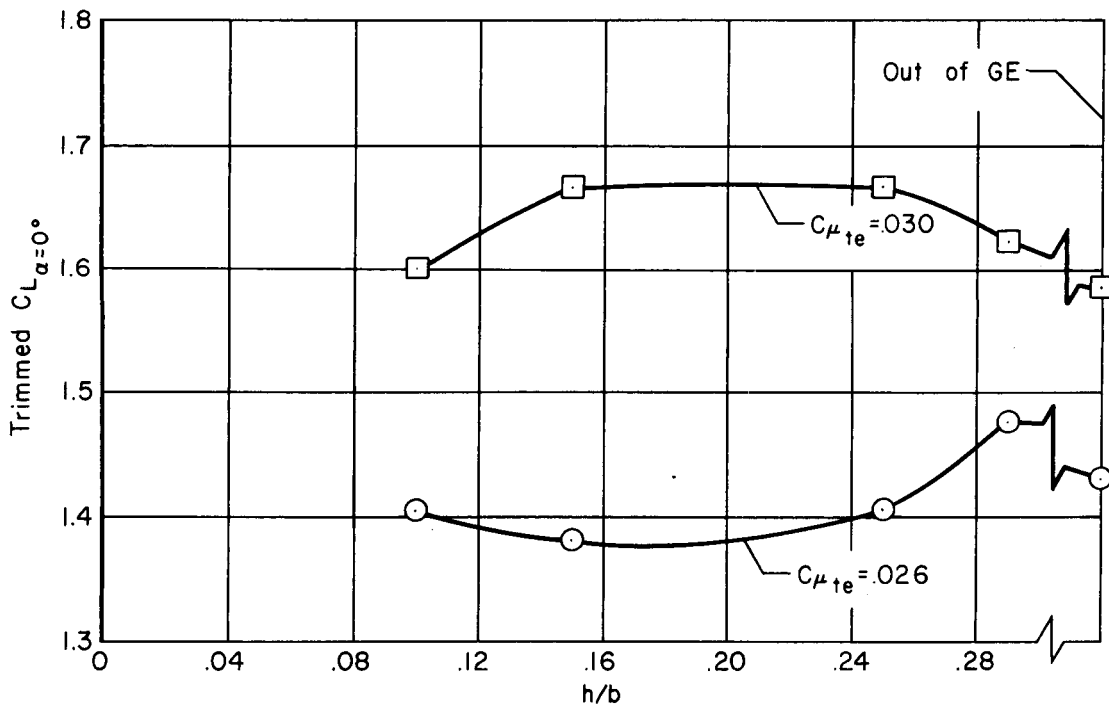
(d) $\delta_f = 50^{O}$ with BLC.

Figure 17.- Concluded.

(a) Normal flap, $C_{\mu_{te}} = 0$.

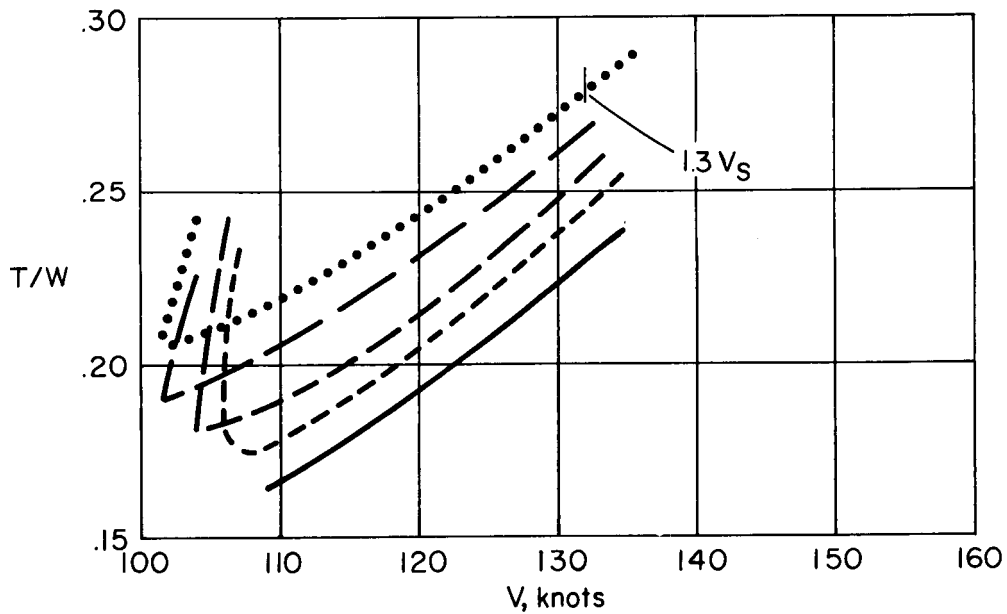(b) Normal flap, $C_{\mu_{te}} = 0.015$.

Figure 18.- Variation with ground proximity of calculated thrust-to-weight ratio required to maintain low-speed level flight; interrupted-span trailing-edge flaps deflected 50°, $W/S = 65$ lb/ft^2, nacelles and pylons on, $\delta_n = 0^\circ$.
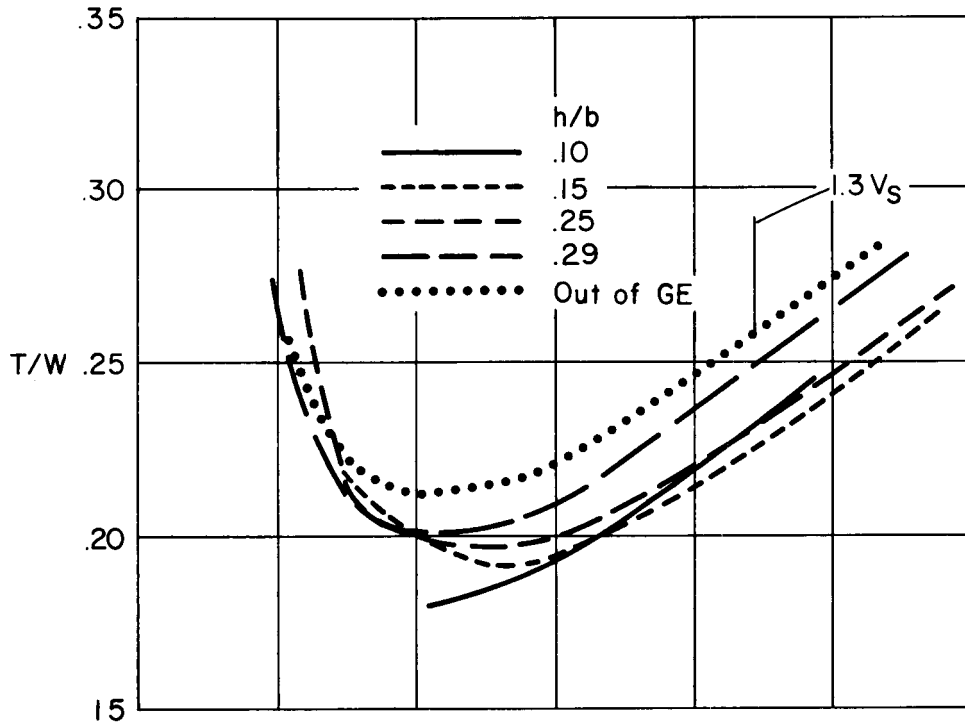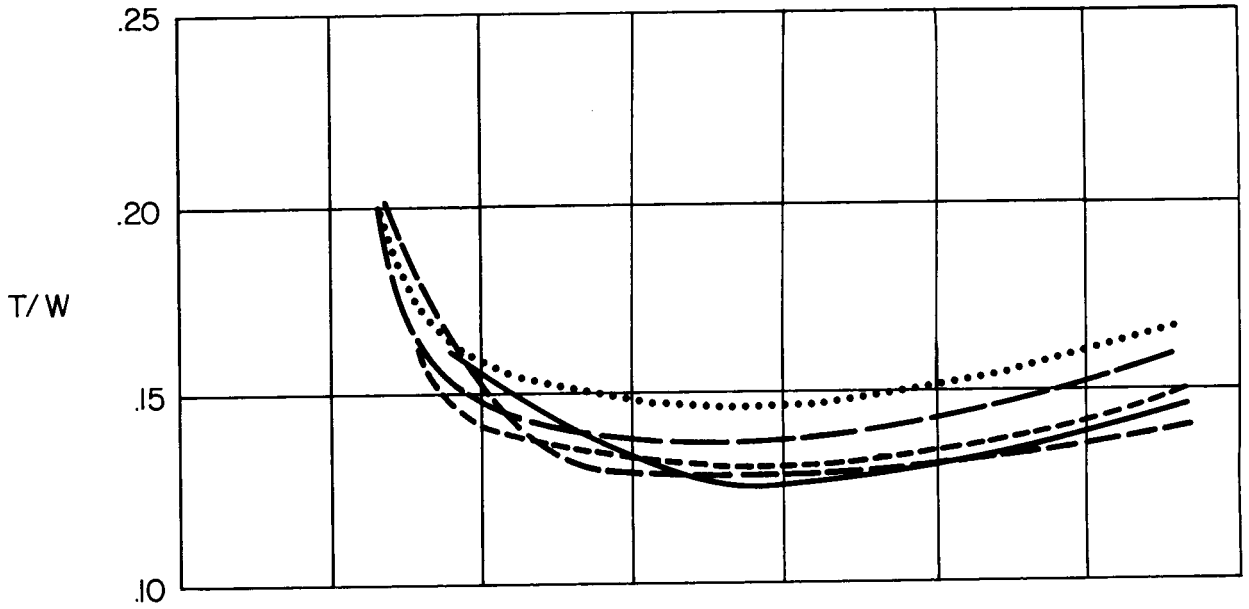
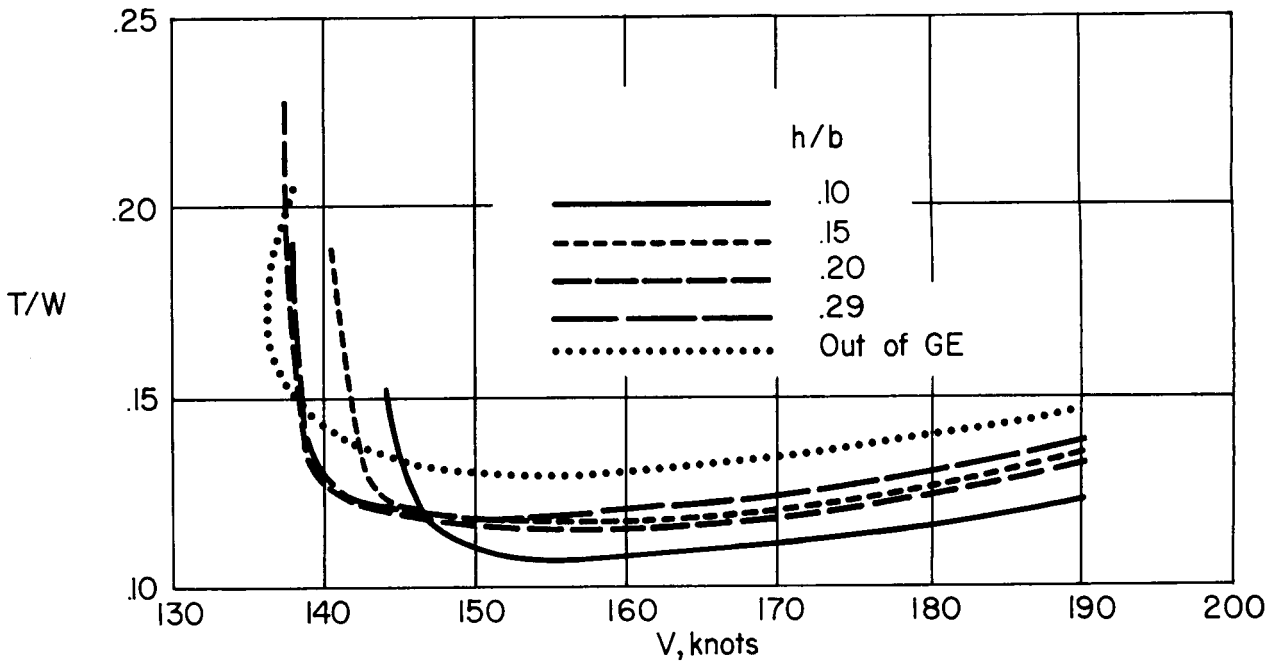(c) Extended chord flap, $C_{\mu_{te}} = 0$.

(d) Extended chord flap, $C_{\mu_{te}} = 0.019$.
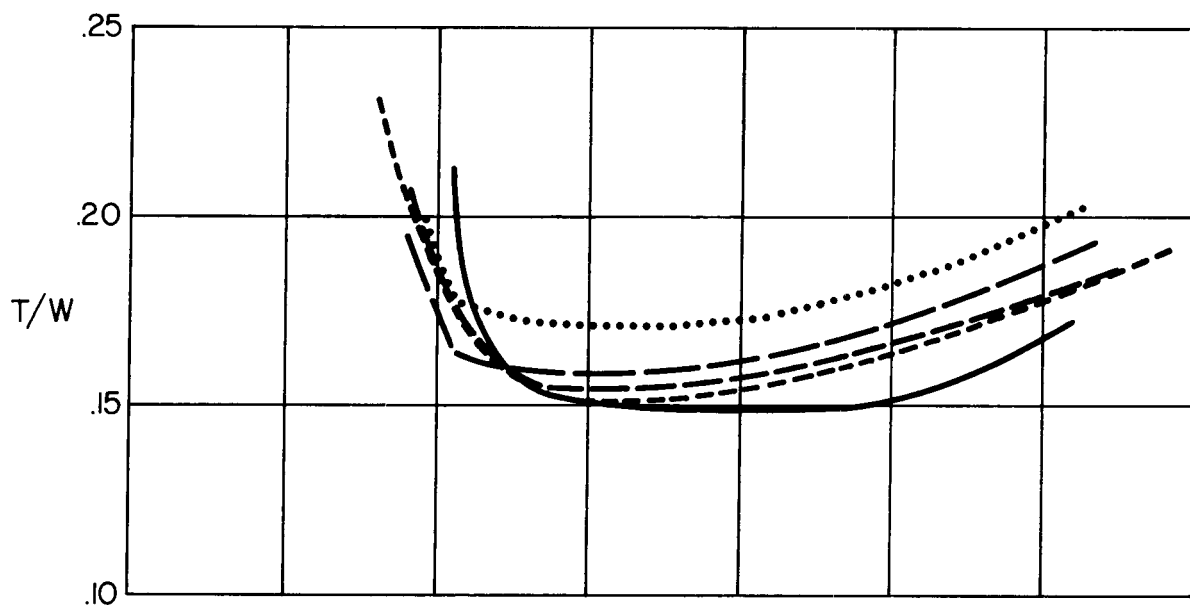
Figure 18.- Concluded.
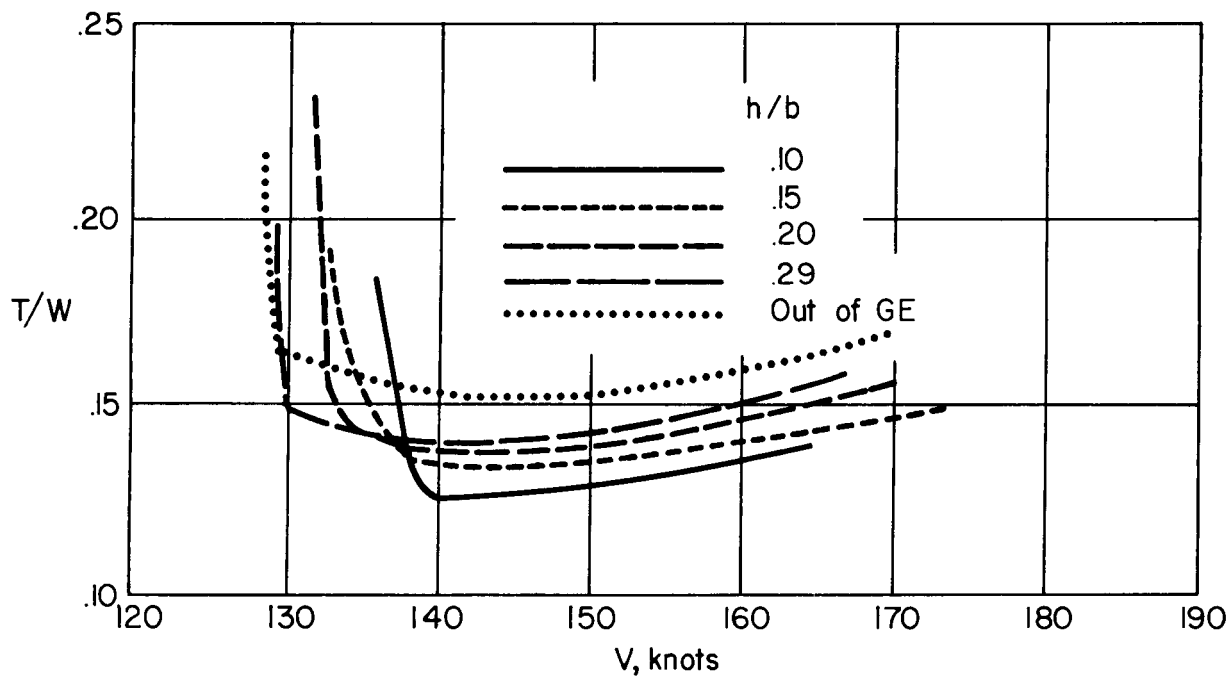
(a) Normal flap, $C_{\mu_{te}} = 0$.

(b) Normal flap, $C_{\mu_{te}} = 0.008$.

Figure 19.- Variation of calculated thrust-to-weight ratio required to maintain low-speed level flight with ground proximity; interrupted-span trailing-edge flap deflected 30°, W/S = 100 lb/ft^2, nacelles and pylons on, $\delta_n = 0^\circ$.

(c) Extended chord flap, $C_{\mu_{te}} = 0$.

(d) Extended chord flap, $C_{\mu_{te}} = 0.010$.

Figure 19.- Concluded.